André Fernando Pinto Lopes
Licenciatura em Engenharia de Materiais

Development of New Cellulose Nanocrystal-based materials with high added value

Dissertação para obtenção do Grau de Mestre em Engenharia de Materiais

Orientadora:	Doutora Susete Fernandes, Departamento de Ciência dos Materiais, Faculdade de Ciências e Tecnologia da Universidade Nova de Lisboa
Co-orientadora:	Professora Doutora Maria Helena Godinho, Professora Associada com Agregação, Faculdade de Ciências e Tecnologia da Universidade Nova de Lisboa

Júri:

Presidente:	Doutor João Veiga, Professor Auxiliar do Departamento de Ciência dos Materiais, da Faculdade de Ciências e Tecnologia da Universidade Nova de Lisboa;
Arguente:	Doutora Ana Baptista, Investigadora Pós-Doc do Departamento de Ciência dos Materiais, da Faculdade de Ciências e Tecnologia da Universidade Nova de Lisboa
Vogais:	Doutora Susete Fernandes, Investigadora Pós-Doc do Departamento de Ciência dos Materiais, da Faculdade de Ciências e Tecnologia da Universidade Nova de Lisboa

FACULDADE DE CIÊNCIAS E TECNOLOGIA
UNIVERSIDADE NOVA DE LISBOA

Maio, 2018

Development of New Cellulose Nanocrystal-based materials with high added value

“Anything worth doing, is worth doing right.”'

-Hunter S. Thompson

Agradecimentos

Gostaria de agradecer ao Departamento de Ciência dos Materiais e ao laboratório CENIMAT|I3N, por me terem dado a oportunidade de desenvolver este trabalho, assim como todos os colaboradores e técnicos de equipamento que neles trabalham, por terem tornado possível a realização atempada deste projecto. Gostaria de agradecer à minha orientadora, Doutora Susete Fernandes, cuja interminável paciência para me ajudar em todos os obstáculos que encontrei durante estes meses tornou este projecto uma realidade. Sem si este documento seria uma sombra do que é, e não estaria neste momento a finalizar estes parágrafos, e por isso, um grande obrigado por fazer o que poucos fariam. Agradeço também à minha co-orientadora, Professora Doutora Helena Godinho, pelo valioso input que deu em vários pontos durante este projecto. Gostaria também de agradecer a todos os professores do fantástico Departamento de Ciência dos Materiais, cujo esforço colectivo me trouxe a mim e a todos aquele que antes de mim chegaram até este ponto. O trabalho de professor é difícil e muitas vezes ingrato, pelo que não posso passar sem vos reconhecer.

O meu percurso ao longo destes longos anos foi preenchido por uma multidão de caras, quase demasiadas para enumerar. Mas nunca fui de recuar de um desafio, francamente:

Benjamim, ainda me lembro quando entrei nesta faculdade, um míudo completamente fechado e com medo de tudo e todos, nesta grande cidade de "gente grande". Obrigado pelo ombro amigo e pelas constantes conversas e temas abordados que só de pensar neles me faziam encolher. Ensinaste-me que policiar os nossos pensamentos é o pior veneno que a nossa alma pode beber, e levaste-me a conhecer pessoas que nunca sonharia existissem. Por isso terás sempre a minha amizade. Obrigado.

Ao fantástico pessoal do mui erudito, e não de todo incrivelmente parvo, Núcleo de Jogos, vocês tornaram toda esta experiência suportável nos piores momentos, e os melhores anos da minha vida nos restantes:
Ao pessoal do EDH, por todas aquelas tardes de sábado perdidas, a rir a bandeiras despregadas, com as ocasionais injecções de sal…
Aos meus amigos do Warhammer, o adepto da Heresia e o adepto dos Imortais, que me acompanharam na minha lenta descida para a loucura e empobrecimento monetário com toda a graça de fanáticos por polistireno…
Aos manos do Discord, pelas horas a fio a dizer porcaria e nada mais que isso. Por tanto objecto virtual encontrado, cartas jogadas e abominações à natureza cravejadas com balas desnecessariamente complexas…
Ao troll e ao homem dos mil hobbies, nunca mudem. Por trazerem sorrisos à minha cara com a ligeireza que consegues trazer a qualquer situação…
Ao historiador/matemático/músico/neckbeard ou lá como te tiveres a sentir quando leres isto, pelas lições, e pela preocupação…
Às instigadoras do Rumikub, a quem ainda devo um jogo ….
Aos meus amigos de Vialonga, que foram um prazer de conhecer e falar todos os dias, e a quem quero continuar a ver durante anos a fio (PS: tragam pizza)…
Aos meus dois gordos (em espírito naturalmente), cuja constante preocupação e contacto deu-me uma segurança e felicidade tal que nunca poderão imaginar. Sei que posso não mostrar, mas vocês verdadeiramente mostraram-me que há amizades que podem durar, e bastou um gelado. Nunca vos esquecerei…

A todos vós…obrigado. Do fundo do meu coração.

O tempo urge e o texto já está comprido, mas há mais caras que eu tenho de reconhecer. À minha madrinha, e todo o pessoal aí em baixo, vocês mostraram-me que por muito sujo que seja um rio, podemos sempre encontrar uma pepita de ouro mesmo abaixo da superfície. Pelo vosso apoio e compreensão, até numa altura

de dor e mágoa, um grande obrigado. Gente mais sábia que eu disse uma vez que uma pessoa só desaparece quando o seu nome escapa dos lábios de alguém pela última vez. Ela nunca será esquecida.

Por fim, porque os melhores e mais importantes para último têm de ficar, ou tal mandata convenções de escrita, não é? Realmente não sou muito bom nisto…

Há alguém a quem eu tenho de agradecer. Alguém que neste momento deve estar a arrepender-se de poder ser associada com uma pessoa que tem as capacidades gramaticais e literárias de uma batata. Uma pessoa que tem estado comigo durante os últimos anos. Thick and thin. Felicidade e tristeza. Sabes quem és. Quando te conheci não era mais que um miúdo parvo. Ainda sou e serei, eternamente, mas sinto que cresci ao teu lado. Conseguiste mostrar me que quando uma lâmpada falha, não se queima a casa. Que quando há um problema, diálogo é a nossa melhor arma. Simpatia, paciência, compreensão, altruísmo, humor e inteligência são apenas algumas das qualidades que me mostraste e continuas a mostrar. Por estes anos de lealdade, ajuda, e todo um mundo de adjectivos que eu francamente estaria aqui o dia todo a enumerar, obrigado. Não te menosprezes nunca. E acredita que vou estar ao teu lado para te lembrar disto durante os próximos anos, enquanto me convenço a mim próprio, que sim, isto é real. Não te vais livrar de mim assim tão cedo…. *Amo-te*.

Por fim, Pai e Mãe. Raúl e Cristina. 23 anos, caminhando para 24. Como a vossa sanidade resistiu ao longo dos anos, às minhas constantes mudanças de humor e crescente stress e ansiedade, nunca saberei. Se professor é ingrato, então Pai e Mãe ainda mais o são, pois é isso e muito mais. Mal consigo passar do coração para o papel o que sinto, porque realmente palavras não servem.
Tudo fizeram para que me educar. Bem e mal. Certo e errado. Eu sou o produto do que vocês tanto se esforçaram para conseguir. Sou alguém com futuro, com confiança, as bases para quem será um dia alguém que viveu uma fantástica vida, se tudo até agora foi alguma indicação. E tudo graças a vocês que com tanto esforço e altruísmo me criaram, sempre pondo o meu bem-estar acima do vosso. Palavras não conseguem expressar o que sinto, pelo que já me estou a repetir. Mas deixo-vos com isto: super-heróis existem. Contos de fada são reais…

Eu, qual anão que sou, nos vossos gigantescos ombros me sento. Agora, e sempre…

Obrigado.

Este trabalho foi financiado utilizando fundos concedidos pela FEDER através do Programa COMPETE 2020 e Fundos Nacionais, através da FCT – Fundação para a Ciência e Tecnologia, ao abrigo do projecto POCI- 01-0145-FEDER-007688 (Referenciar UID/CTM/50025) e através de M-ERA.NET, uma rede financiada pela UE, para o projecto 2/0007/2016 – CellColor.

Abstract

Stimuli-responsive materials present incredible versatility, since they adapt their properties to external stimuli. If derived from nanomaterials as cellulose nanocrystals (CNC), originated from the world's most abundant natural polymer, it can widen their scope to a new range of applications.

The goal of this work involved the synthesis and characterization of new CNCs functionalized with a chromophore with photoresponsive properties, to produce a compound with tuneable and adaptive characteristics that can respond to external stimuli.

Acid hydrolysis, using sulphuric acid, was performed on cotton filter paper and CNCs were obtained with an average length of 209±47 nm. The reaction of the CNCs with 4-(4-Methoxyazobenzene-4′-yloxy)butyric acid (Azo), yielded a new Azo-CNC material with a degree of substitution of approximately 0.05, without compromising its initial structure at the nanoscale. Despite having low incorporation, the azo moiety confers higher thermal stability, with an increase in the initial decomposition temperature of 110ºC.

Filter paper, CNC and Azo-CNC were analysed through AFM, FTIR, XRD, DSC-TG and elemental analysis. Wettability essays were also performed on CNC and Azo-CNC films, obtained by solvent casting. The preliminary results showed that the azo-groups increase the hydrophilicity of the film and give rise to a superhydrophilic material, with a remarkable bending response to water.

Materials such as this represent promising applications of CNCs and are options for tuneable, cost-effective and sustainable solutions for the production of advanced stimuli responsive structures.

Keywords: Cellulose nanocrystals, azobenzene chromophore, stimuli responsive materials, superhydrophilicity

Resumo

Devido à adaptabilidade das suas propriedades a estímulos externos, materiais com resposta a estímulos propiciam um grande número de aplicações criativas na nanoescala, especialmente se produzidos a partir de nanomateriais existentes. A celulose nanocristalina (CNC), um material derivado do polímero natural mais abundante do planeta, é um desses materiais com potencial.

O objectivo deste trabalho prendeu-se com o desenvolvimento e caracterização de uma nova CNC funcionalizada com um cromóforo com propriedades foto-responsivas, pretendendo-se a produção de um material de características moduláveis e adaptáveis com possível resposta a estímulos externos.

Papel de filtro de algodão foi utilizado como material de partida para uma reação de hidrólise ácida, produzindo uma suspensão de CNC com um comprimento médio de nanopartículas de 209±47 nm. As nanoceluloses preparadas foram posteriormente utilizadas em reação com ácido 4-(4-Metoxiazobenzeno-4′-iloxi)butírico (Azo), originando um novo material, denominado Azo-CNC. Um grau de substituição médio de 0.05 foi conseguido, sem comprometer a estrutura inicial da CNC à nano-escala. Apesar da incorporação relativamente baixa de cromóforo, a funcionalização concedeu uma melhor resistência térmica à estrutura celulósica, resultando num aumento na temperatura de decomposição inicial de 110 ºC.

Amostras de papel de filtro, CNC e Azo-CNC foram analisadas através de FTIR, DRX, XRD, DSC-TG e análise elementar. Em adição, foram levados a cabo testes de molhabilidade em filmes finos de CNC e Azo-CNC, obtidos pelo processo de evaporação de solvente. Resultados preliminares mostraram que a hidrofilicidade do Azo-CNC aumentou consideravelmente face às CNC. Os filmes preparados inclusivamente demonstraram propriedades superhidrofílicas, bem como uma resposta mecânica de flexão considerável em resposta a água.

Materiais como este apresentam aplicações promissoras de CNC e fazem parte de um grupo de soluções versáteis, eficientes e sustentáveis para a produção de materiais avançados responsivos a estímulos.

Palavras-chave: celulose nanocristalina, cromóforo azobenzeno, materiais com resposta a estímulos, superhidrofilicidade

Table of contents

List of tables

List of figures

Abbreviations

AGP	Anhydroglucopyranose
TEMPO	Tetramethylpiperidinyloxyl
HPC	Hydroxypropyl cellulose
MFC	Microfibrillated cellulose
CNC	Cellulose nanocrystals
R or R’	Functional group
Azo	Azobenzene derivative
APC	Acetoxypropylcellulose
ATR-FTIR	Attenuated total reflectance Fourier-transformed infrared
DSC	Differential scanning calorimetry
TGA	Thermogravimetric analysis
XRD	X-ray diffraction
AFM	Atomic force microscopy
SEM	Scanning Electron Microscope
$\overline{DS}$	Average degree of substitution

1. Introduction

In a world that is increasingly environmentally conscious, new and sustainable solutions for long-standing problems are ever more in demand, so we begin to look towards different materials, such as cellulose, considered the most abundant naturally-occurring polymer, being the main component of plant cell walls. Research on this material is constant, and presents an interesting set of properties, like non-toxicity, high resistance, hydrophobicity, yet tendency to swell with water, biocompatibility and biodegradability, low cost and renewability. It is chemically highly versatile resulting in a variety of derivatives that can be made from it. Each cellulosic derivative presents differing characteristics [1] allowing its use in diverse applications and research that ranges from electronics [2] to pharmacy [3]. Its place in industry is also notable, such as the production of paper, which, by itself, put into circulation around 400 million tons of paper and cardboard derivatives worldwide [4].

Specifically, cellulose, or polyanhydro-β-D-glucopyranose, is a polydisperse, linear, macromolecule of relatively high molecular weight, classed as a polysaccharide. Its specific properties vary with its source, so it is possible to tailor the material to its intended use, even before refinement processes [5]. Cellulose chains are believed to normally organize themselves into interwoven amorphous and crystalline regions, resulting in a semi-crystalline material, in which the amorphous regions are, naturally, more susceptible to chemical attack than the crystalline ones [5]. Individual cellulose molecules organize themselves into clusters called protofibrils, which further bundle into microfibrils, whose aggregates we designate as the often mentioned cellulose fibres [6]. The monomer of these macromolecules is cellobiose and is composed of two anhydroglucopyranose (AGP) units twisted 180º around a β-1,4 linkage, as shown in Figure 1.1 [5]. In addition, every cellobiose unit possesses six OH groups, located in the carbons numbered as 2, 3 and 6, which due to their position within the chain, and the possibility of intra and intermolecular hydrogen bonds, present different reactivity from each other, with the group present in C6 being the most reactive [7].

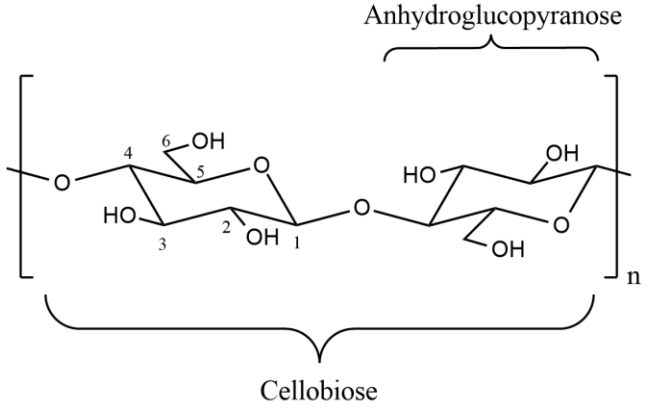

Figure 1.1 – Schematic representation of the chemical structure of the cellulose monomer and its constituent anhydroglucopyranose units, twisted around the connective β-1,4 linkage.

Depending on the intended use for the produced cellulose, it may require that its surface properties be altered and to this end, reactions with the intended outcome of replacing its hydroxyl groups with other groups are employed, in what is called a functionalization. For example, commonly used methods include oxidation, with compounds such as TEMPO (tetramethylpiperidinyloxyl) to introduce carboxylic or aldehyde groups or hydrolysis with sulphuric and phosphoric acids [7], also esterification and etherification, in which a functional group of the respective type is coupled to the chain [9]. Processes like these and others allow the production of a diverse set of cellulose

derivatives, such as hydroxypropyl cellulose (HPC), a water-soluble derivative that is commonly used in industry as an emulsifier and that is produced via etherification [10]. Another example is the carboxymethyl cellulose (CMC), which shares HPC's applicability in the food, cosmetic and pharmaceutical industries [11]. It is also possible to alter or produce cellulose with different sizes, by using diverse methods: microfibrillated cellulose (MFC), nanometer-long fibrils made via mechanical processes with/without pre-chemical treatment [12][1]; bacterial nanocellulose (BNC), utilizing bacteria such as the *Gluconacetobacter* genus and glucose to produce nanofibers in a form of solid film [1]; and cellulose nanocrystals (CNC), rodlike structures produced through acid hydrolysis [1][13].

1.1. Cellulose Nanocrystals

In 1949, Rånby et al. were successful in reducing cellulose fibres into a stable suspension of colloidal nanometer-wide crystals using acid hydrolysis [14], and research on this material has been constant ever since, with special attention in the last decade [1][6][15]. The semi-crystalline structure of cellulose lends itself to this refinement process, wherein the amorphous areas of the cellulose fibres are attacked by the acid of choice, and if done correctly, only leaving behind the crystalline sections [6], referred to as crystallites, which typically possess a degree of crystallinity over 90% [5]. The exact size and shape of these crystals vary with both the source of the cellulose and the parameters of the reaction, for instance, with longer reaction times and increased acid concentrations resulting in an reduction of size and sample distribution [16]. From cotton, microcrystalline cellulose and wood pulp a product with a small size distribution, high crystallinity and dimensions around 5-15 nm wide and 90-120 nm long, can be obtained. If other sources are used like algae and bacteria, more polydisperse and bigger whiskers, with average widths of 5-60 nm and lengths of 100 nm to upwards of several micrometers [1][17] are obtained. However, CNC have a natural tendency to aggregate, and do not produce stable suspensions. To counteract this acids such as sulphuric and phosphoric are chosen for the hydrolysis process, ensuring that the resulting crystallites possess a surface charge that will minimize their aggregation [5].

Like other cellulose derivatives, CNC present the capacity to form a lyotropic, cholesteric liquid crystal phase [1][18]. This phase in CNC was originally described in 1992 by Revol et al. [19], and due to the continued efforts of this group, but not limited to, much groundwork for future research in the area was set down. The basis towards the formation of the liquid crystal phase is that, when CNC is in an aqueous suspension, if aggregation or precipitation does not occur and a critical concentration is reached, an anisotropic phase will be formed, where the proximity of the CNC will cause them to self-align along a structure that is better simplified as a "pseudo-layered" structure. In each "layer" the CNCs will arrange themselves in average around an axis called the director axis, **n**. In the next layer **n** will be tilted at an angle in relation to the previous one, leading to a shift on the director axis from layer to layer along a perpendicular **z** axis, forming a helical shape with axis **z** [5][20]. This phase presents intermediate behaviour between solids and liquids, maintaining long-range spatial order, without short-range order, varying refraction indexes within the material, depending on the direction of light propagation, which is called birefringence. If this cholesteric structure is preserved while the solvent evaporates the solid film produced present very interesting optical properties such as structural coloration (iridescence), selective light reflection and transmission of polarized light, mimicking for instance the exo-cuticule of certain insect species [5][18][20].

CNC have several useful characteristics that build-up on the advantages of cellulose, including, low abrasiveness, lightweight, high aspect ratio, high surface area, and superficial hydrophilia [5][7]. CNC are widely researched in a variety of fields. For example, Chaichiet al. managed to improve a previously known edible biofilm, Pectin, with CNC as reinforcement, with an increase

of 84% in tensile strength and a 40% reduction of water permeability, while maintaining its biocompatible properties, opening it to possible applications in green and sustainable food packaging [21]. Other applications emphasize its chemical versatility, such as the work presented by Lopez et al., who successfully grafted fuellerene derivatives into functionalized TEMPO-CNC. The authors showed that these new hybrid compounds can be used in the production of singlet oxygen, a highly reactive form of the element that is used in photodynamic treatment of cancer cells due to its toxicity, which makes them a promising candidate for cancer treatment [22].

1.2. Response to external stimuli

Given the increasingly complex demands made for new applications one option might pass by the development of stimuli-responsive, or "smart", materials. Their principle of operation boils down to the following: when subject to a specific stimulus (or stimuli) to which they are able to respond to, they alter one or more of their properties. Possible stimuli that could trigger a reaction include temperature, light, mechanical solicitation and humidity, among others [23]. A multitude of materials with this kind of response can be found, such as piezoelectric [24], shape memory [25] and self-healing [26]. Given the characteristics mentioned above for cellulose and derivatives, they are good candidates for functionalization into a "smart" material [27]. Geng et al. reported a soft cellulose-based motor driven by humidity, which utilized a loop of HPC film, derived from its lyotropic aqueous phase, to generate motion when one extremity was exposed to humid air and the other to dry air [28]. More recently, Wang et al. demonstrated that thin solid films of MFC, derived from isotropic suspensions, possess a highly sensitive response to localized increases in humidity, bending when a humidity difference across the film is introduced, and unbending when the stimulus is removed, in just a few seconds [29]. Within stimuli-responsive materials attention has also been given to chromophores, compounds with very interesting photoresponsive properties, and their role in the functionalization of polymer networks [30][31].

1.3. Chromophore-functionalized polymer networks

Chromophores are a type of stimuli-responsive molecule that possess unique photoresponsive properties, responding to specific wavelengths dependent on the compound used. Stilbene, spyropyran, fulgides and azobenzenes are examples of these type of compounds. Out of these possibilities, azobenzenes (Azo) have drawn a lot of interest, due to their properties, such as good stability, low flammability, bright coloration and quick reversible photoresponse. Azobenzenes are a type of compound composed by two phenyl rings linked by a N=N bond, with the possibility of a variety of functional groups (R, R') extending from the rings. These compounds can undergo photoisomerization from trans to cis isomers, as shown in Figure 1.2 [30]

In 2001, Ichimura et al. showed that when a monolayer of a low molecular weight compound bearing azobenzene-moieties was locally irradiated with an asymmetrical light, creating a gradient of isomerization, induce movement in liquid droplets. The authors were able to control the movement of the liquid particles as long as the stimulus was maintained [32]. Interest has also been shown in the advantage of functionalization of liquid crystal elastomers with this type of photochromic molecules [33] such as the work by Ikeda et al.. The authors successfully functionalized polymeric liquid crystal gels with Azo-moieties and noted reversible photosensitive responses in the form of bending when the elastomer was irradiated [34]. Recently, Koçer et al. developed novel azo-benzene based liquid crystalline polymer networks to produce films that could undergo photoresponsive microscale topographic variations as well as changes in roughness at the nanoscale, which are factors that were shown to influence cell speed and migration patterns. Opening its use in the field of cellular regeneration and therapy [35]

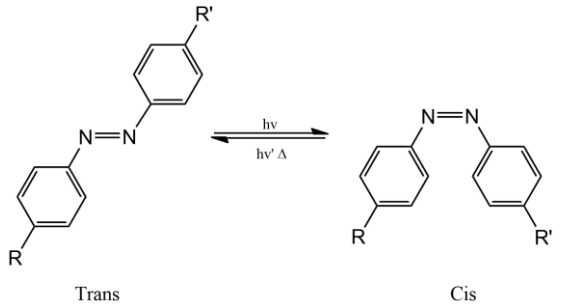

Figure 1.2 – Schematic representation of the photoinduced *trans*-to-*cis* isomerization under light irradiation of azobenzene compound.

Among polymers, cellulose shows itself to be a very promising candidate for functionalization with azobenzenes, given its previously stated versatility and cost-effectiveness. In 2001, pioneer work was conducted by Yang et al., reporting the synthesis of novel Azo-modified cellulose (Azocellulose) polymer and the authors confirm that despite being linked to the cellulose polymer chains the *cis-trans* photoisomeration of the azobenzene moieties occurs [36]. Hu et al. successfully functionalized hydroxypropyl methylcellulose with an Azo-moiety (Azo-HPMC). Starting from a water soluble material (HPMC) the authors noted that the variation of the degree of substitution in the polymer chain affected its water solubility, with higher substitution resulting in an insoluble compound [37]. Later, in 2010, Lizu et al. prepared two thermotropic liquid crystal ethylcellulose networks, each modified with a different azobenzene compound, and after functionalization maintained their mesomorph phases. However, depending on the chromophore used, a different liquid crystal texture was identified, with columnar and smectic phases being present. Photochromic properties linked to the azobenzene moieties were also identified [38].

Pinto et al. in 2011 successfully functionalized the thermotropic cellulose derivative, acetoxypropylcellulose (APC), with an azobenzene compound that could respond to UV irradiation. The authors reported that this material underwent a reversible *trans–cis* isomerization of the azo moiety when subjected to alternating cycles of UV and visible light irradiation, resulting in reversible changes to the surface wettability of the produced thin films. This was confirmed due to a change in wettability, from hydrophobic (water contact angle of 125° in *trans* conformation), to a much less hydrophobic surface (water contact angle of 90° in *cis* conformation). This behaviour was thought to be consequence of the low mobility constriction of the Azo- moieties due to the flexibility characteristic derived from the liquid crystalline behaviour of this cellulosic derivative [39]. Following, Huang et al. described analogous photoresponsive wettability behaviour of functionalized azobenzene-HPC, a hydrophilic cellulosic derivative, reporting a wettability transition from a hydrophilic to a more hydrophilic state, and showing that this transition was influenced by the degree of azobenzene substitution. Measured static contact angle variation increased from 4º to 7º when the average degree of substitution ($\overline{DS}$) of azo-moieties in the polymer chains rises from 0.45 to 1.19. The authors posited that the observed wettability changes were partly derived from the exposure of N=N bonds due to the photoisomerization of the chromophore into the *cis* form, as this double bond can form hydrogen bonds with water, leading to a more hydrophilic material [40]. Fernandes et al. more recently exposed that the thermotropic Azo-APC described above could manifest different wettability properties depending on the nanostructures formed, determined by film deposition conditions. In this study, Azo-APC Langmuir-Blodgett multilayer films, filaments and lamellas were produced, and the authors found that while lamellar structures maintained the photoresponse expected of Azo-APC, both multilayer and filament films exhibited a hydrophilic behaviour, with little to no changes caused by UV light irradiation. This implies that chromophore response is dependent on

the nanostructure of the modified material, with certain arrangements, like the Langmuir-Blodgett films, trapping or otherwise restricting movement of the azo-moieties [8]. All these results show that this cellulosic functionalized derivative could have multiple applications, opening the possibility to obtain coatings from just one cellulosic derivative with diverse wettability behaviour, and that also can be changed when subjected to light irradiation.

From combining the advantages of chromophore-functionalized polymer networks and the interesting properties of cellulose nanocrystals, which possess the added benefit of potential liquid-crystal properties, comes the inspiration for this work that to the best of our knowledge has not been done yet, that could lead to versatile new materials for innovative applications.

2. Materials and Methods

2.1. Production of Cellulose Nanocrystals

Whatman No. 1 filter paper from cotton origin, was cut into 3x4 cm pieces, and then shredded using two food processors (La Moulinette A320R1 chopper from Moulinex® and a smaller Basic Line brand coffee grinder) into fibres of approximately 25±6 µm in diameter (determined from 50 measures done with ImageJ version 1.8.0_112 from fibers observed by polarized optical microscopy, see supporting information Figure 6.1). Sulphuric acid (98% purity), purchased from Sigma-Aldrich was used after dilution to 64.0 % (w/w). Amberlite IR120 Hydrogen Form strong cation resin (from Sigma-Aldrich) was used after extensive washing. Spectra/Por® cellulose dialysis membrane was purchased from Spectrum Labs and used after washing.

Typically, CNC were prepared, by acid hydrolysis of the filter paper fibres described above with sulphuric acid (64 % (w/w)) at 45 ˚C for 45 minutes, according to an adaptation of the method described by Gray et al. [41]. The resulting suspension was quenched in 10 x the initial volume with ultrapure water (Elix® Advantage 3 Water Purification System) and washed with ultrapure water daily for 3 days. The suspension was further washed using centrifugation (20 minutes cycles at 12000 rpm) until the CNC suspension remained stable with no sedimentation. Excess of sulphuric acid was then further removed with dialysis against ultrapure water, until a constant pH of 5.5 was reached (2-3 weeks). Afterwards, a ionic exchange resin was added to protonate the suspension, according to the method of Beck et al. [42], performing six batch treatments of 30 minutes each, at a ratio of 5g of resin per gram of CNC. The resin was then removed via filtration, using a 22µm mesh (Whatman No. 541). Yields around 30% were obtained. The treated CNC suspension was then freeze-dried at 0.1 mbar and -45 ºC for 4 days, using a Zirbus Technology VaCo 2.

2.2. Azo-CNC synthesis

THF (Tetrahydrofuran, ACS, Fisher Scientific), pre-treated with sodium, was dried through reflux under sodium before use. 4-DMAP (4-Dimethylaminopyridine) and DCC (N,N'-dicyclohexylcarbodiimide, Fluka Chemika) were used as received. The azo derivative, 4-(4-Methoxyazobenzene-4′-yloxy)butyric acid already available as described by Pinto et al. [39], was kindly given and used as received.

The CNC's functionalization reaction occurred in heterogeneous medium and was adapted from Pinto et al. [39]. Typically, freeze-dried CNC (0,5 g) were suspended in dry THF (60 ml/g), and the resulting suspension was then cooled in an ice bath, keeping it at around 3º C during the next steps. 4-DMAP (0.021 g) and the azo derivative (0.143 g) were added directly, under stirring, while DCC (0.25 g) was suspended in dry THF (approximately 20 ml) and added dropwise. Afterwards, the suspension was left under stirring (200 rpm) at room temperature for approximately 140 hours. After this period, the suspension was washed by centrifugation in 20-minute cycles at 12000 rpm, adding fresh THF between cycles, until the supernatant did not evidence traces of azo derivative. The suspension was dried under vacuum at 50 ºC for approximately 48 hours until constant weight.

2.3. Characterization

Aqueous CNC and Azo-CNC suspensions, each 4 g at 4% (w/w), were prepared by sonication using a Hielscher UP400S Ultrasonic Processor (460 W, 24 kHz), at 30% power with 0.2 of the cycle of for 10 minutes. Films were prepared through the solvent evaporation method by placing the suspensions in a polysterene Petri dish (35 mm) at room temperature and under visible light.

Elemental analysis, Fourier-transformed infrared (FTIR), scanning calorimetry with thermogravimetric analysis (DSC-TG), x-ray diffraction (XRD), polarized optic microscopy (POM) and general photography were performed on samples of both CNC and Azo-CNC. Standard parameters were used, and can be found, along with the equipment used, in the supplied supplementary information section 6.1.

Nanocrystal suspensions of 0.01% (w/w), sonicated at 85% power, with 0.8 of the cycle for 10 minutes, were deposited onto a mica (Muscovite Mica, V-5 from Electronic Microscopy Sciences) substrate and observed by atomic force microscopy (AFM) using an Asylum Research MFP-3D Standalone System in tapping mode, with Olympus AC160TS silicon AFM probes and the images used to obtain CNC and AZO-CNC size and aspect ratio with the Gwyddion 2.50 software (see supplementary information section 6.3). The same suspensions were observed through scanning electron microscopy (SEM), using Carl Zeiss Auriga crossbeam (SEM-FIB) workstation instrument equipped with a Dan Oxford energy dispersive x-ray spectrometer, and pictures taken with an acceleration voltage of 2 kV and aperture size of 20 μm. The suspension was deposited on an ultrathin carbon film supported by a lacey carbon film on a 400 mesh cooper grid (from TEDPella, Inc). Size and aspect ratio were obtained using ImageJ version 1.51j8 software (see supplementary information section 6.3). Cross-sections of CNC and Azo-CNC films, coated by a 30 nm layer of conductive carbon using a Q150T ES Quorum sputter coater were observed by SEM and the pitch values measured using the ImageJ software (refer to supplementary information section 6.4).

A thermal stabilization treatment of film samples was done based on the work described by Dankovich et al. [43]. Study of ideal treatment parameters was done at several temperatures and times, with the optimal conditions determined to be 15 minutes, at 105 ºC for CNC films and 150 ºC for Azo-CNC. Wettability tests were done using a Dataphysics Contact Angle System 20 OCA, ultrapure water droplets of 2-5 μl were deposited on top of the casted films, in diverse humidity environments of 30-40% or 90-95% relative moisture (saturated atmosphere). Video was acquired using the in-built camera and static contact angle measurements were done with the bundled SCA20 software, with the Young-Laplace method. These tests were repeated a total of 15 times for CNC samples and 30 times for Azo-CNC samples in different places or parts of the samples. Additional wettability essays were then performed on two samples, first with a control test as described above, followed by a 20 min relaxation period, and a 20 min period of UV exposure (with a 4W, 365 nm source), after which a new wettability essay was done and the response times measured.

3.Results and Discussion

This work focuses on the production and characterization of a novel, stimuli-responsive material, brought forth from the functionalization of the remarkable nanoscale cellulose derivative, CNC, with a stimuli-responsive azo-derivative.

The first part of the work involved the synthesis of cellulose nanocrystals from filter paper and the second its functionalization, with structural, morphological and chemical characterization performed on the starting material, nanocrystals and the resulting novel polymer. Solvent-cast films of both CNC and Azo-CNC were then prepared, and their wettability and water-response determined.

The water-induced response behaviour displayed by the new Azo-CNC was investigated, with films displaying both remarkable hydrophilicity, reaching superhydrophillic status, as well as a, to the best of our knowledge, novel bending response for a CNC-derived film.

To facilitate the presentation and discussion of the preparation of the CNC and Azo-CNC as well as its characterization all the results will be presented together, including those of the starting material, the filter paper.

3.1. CNC production and Functionalization with Azo moieties

Acid hydrolysis of filter paper was done, as described above and according to scheme (1) presented in Figure 3.1, and stable CNC suspensions were successfully produced, with yields of around 30%, consistent with literature for the parameters used [44]. The suspension stability can be attributed to the sulfate half esther groups ($–OSO_3^-$) introduced into the polymer chain during hydrolysis, grafting them in the place of substitutable –OH groups [44], as those of linked to the carbon number 6 (Figure 1.1). Additionally, these CNC are capable of presenting liquid crystalline phases, as evidenced by the colour and birefringence exhibited in suspension (see supporting information Figure 6.2).

The CNC were then functionalized, with a catalysed substitution of the available –OH groups in the cellulose chains, by way of grafting azo moieties, employing a coupling agent, according to scheme (2) represented in Figure 3.1. The 140 h reaction time was optimized after previous attempts failed to produce CNC with a measurable amount, by means of elemental analysis, of Azo incorporation.

The chemical analysis of the new cellulosic materials as done by ATR-FTIR and the spectra of filter paper (a), CNC (b) and Azo-CNC (c) are depicted in Figure 3.2. In the three spectra, all the characteristic IR absorption frequencies attributed to the functional groups of cellulose can be seen, such as the strong band at 3334 cm^{-1} attributed to the stretching vibration of the O–H bond, the C-H stretching at 2900 cm^{-1} and C-O stretching at 1054 cm^{-1}, along with a peak at 1650 cm^{-1} attributed to the O-H bending. All assignments are in accordance with the observed values found in the relevant literature [45]. Additional peaks pertaining to the substituted sulphate groups derived from the acid hydrolysis of the filter paper can also be identified in the 860 cm^{-1} to 780 cm^{-1} range (S-O stretching) in both nanocrystal samples (Figure 3.2 c) and d)) and are in accordance to what is described in the literature [45]. In the Azo-CNC sample new peaks can be observed: the peak at a wavenumber of 1500 cm^{-1} (N=N) is associated with the vibration of the nitrogen double bonds, at 1739 cm^{-1} is assigned to the presence of a carbonyl group (C=O) and the peak at 1598 cm^{-1} is attributed to the stretching vibration of the carbon double bond (C=C) of the aromatic in the azo moiety, all of which are present in the azo-derivative used in the reaction [39][40], confirming presence of azo-moieties in the AZO-CNC samples.

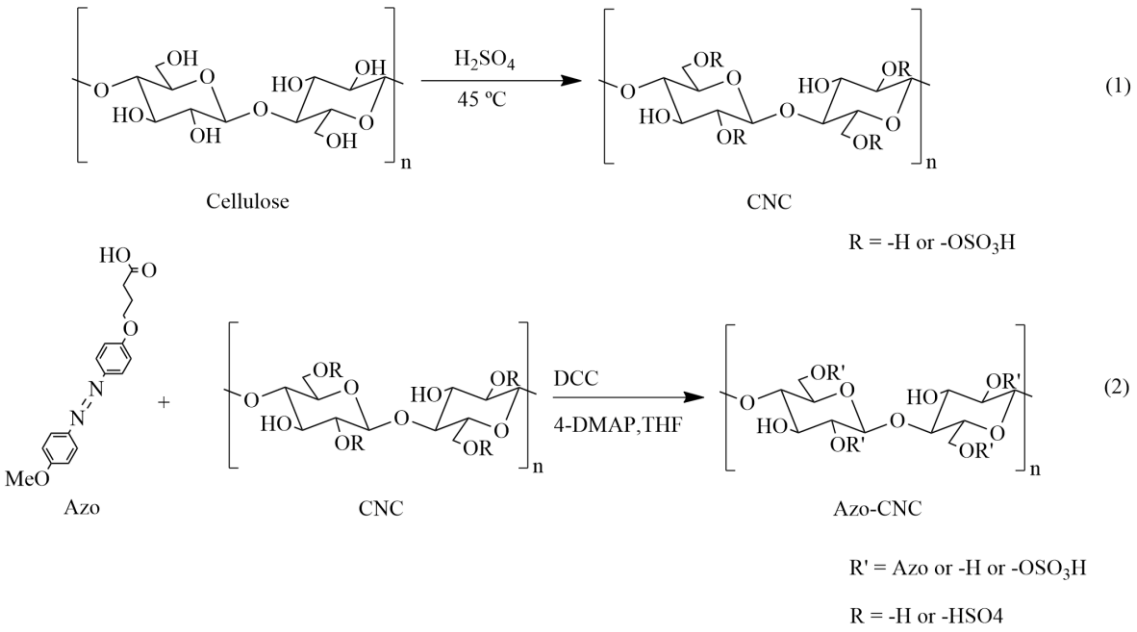

Figure 3.1 – Schematic of the synthetic route used to yield CNC (1) and Azo-CNC (2)

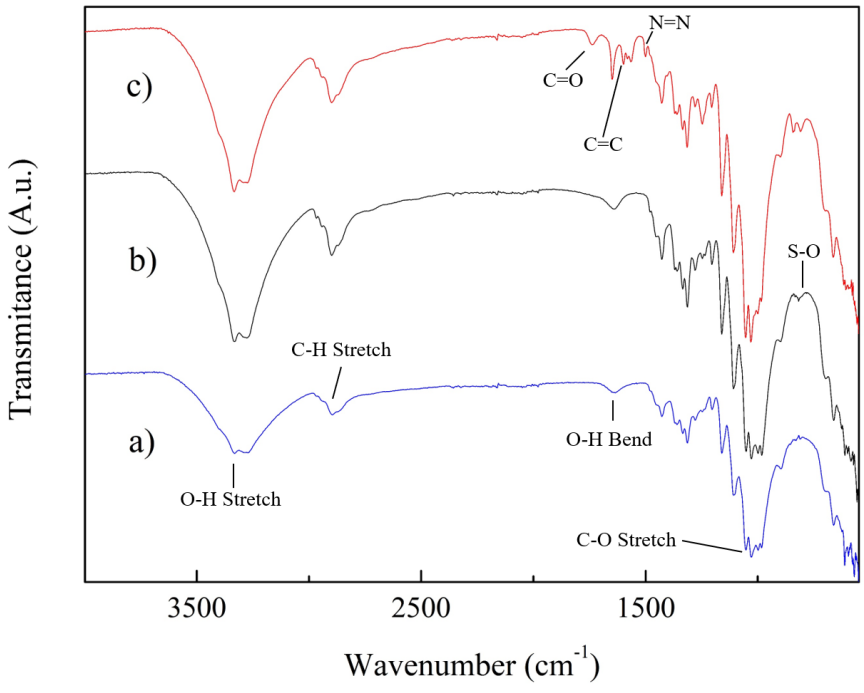

Figure 3.2 – FTIR spectra of a) Filter Paper, b) CNC, c) Azo-CNC showing the characteristic transmission bands of cellulose and the presence of azo-derivative used for its functionalization.

An estimation of the amount of sulphate and Azo-groups attached to the CNC chains can be ascertained from elemental analysis. Performed in at least duplicate, the carbon, hydrogen,

nitrogen and sulphur contents of the samples were determined, and are represented on Table 3.1 (refer to supplementary information section 6.1).

Observation of the elemental analysis results show levels of carbon and hydrogen in filter paper and CNC that are in accordance with the values found in the literature for this type of filter paper and the CNC derived from it [46]. The results observed for the pristine CNC are lower than those predicted for pure cellulose. This might be due to the presence of hard-to-remove water on the high surface area of the cellulose nanocrystals. The presence of sulphur on both nanocrystal samples confirms the incorporation of sulphate half-ester groups during the acid hydrolysis process.

In the Azo-CNC sample a nitrogen content of 0.83% is obtained, and an increase in the carbon and hydrogen levels can be seen confirming the presence of azo moieties, which possess an nitrogen double bond (N=N), characteristic of the azobenzene compound [36][46]. The sulphur content observed on Azo-CNC is slightly higher than those of the CNC, and this difference can be linked to the heterogeneous nature of the tested samples, however, they are of the same order of magnitude.

Table 3.1 – Elemental Analysis results

Sample	Carbon (wt%)	Hydrogen (wt%)	Nitrogen (wt%)	Sulphur (wt%)	Oxygen* (wt%)
Pure cellulose Predicted values[46]	44.44	6.18	----------	----------	49.38
Filter Paper	41.9	6.5	----------	----------	51.95
CNC	41.5	5.8	----------	0.35	52.35
Azo-CNC	43.5	6.4	0.83	0.45	48.82

*Values obtained by mass difference

Using these values, the incorporation of the above-mentioned sulphate half esters can be determined. The method described by Hamad et al. [44] was chosen to return the value of the $\overline{DS}$ of $–OSO_3H$ per 100 AGP units (n):

$$n = \frac{100 \times 162.141 \times S(\%)}{3206.6 - 80.063 \times S(\%)}$$

With S(%) being the sulfur content measured by elemental analysis. The value of n for pristine CNC is 1.68 $–OSO_3H$ groups per 100 AGP units. These values are slightly lower than those observed by Huang, et al. for the same hydrolysis time and temperature [46]. This might be due to the difference in the preparation of the starting material, that in our case give rise to fibres with irregular sizes. In the Azo-CNC samples, the value is 2.30 $–OSO_3H$ per 100 AGP units.

In order to determine the correct $\overline{DS}$ of the azo-moieties per 100 AGP units, we must consider that the Azo-CNC structure already has $–OSO_3H$ substituents incorporated into it. Therefore, the value for the correct molar mass (M_{COR}) of an AGP unit must be determined with the following equation:

$$M_{COR} = M_{cellulose} + M_{OSO_3H} \times \overline{DS_S} = 162.141 + 80.063 \times \overline{DS_S}$$

Using the calculated value for $\overline{DS}$ per AGP unit (n/100) of 0.023 gives us M_{COR} of 163.982 g/mol. To determine the average azo-moiety substitution, the method of Huang et al. [46] was used, with a slight adaptation to include the new calculated value for the average AGP unit:

$$N = \frac{\overline{DS}_{AZO} \times 14 \times x}{M+(\overline{DS}_{AZO} \times MS)}$$

Where M is the above calculated corrected molar mass for an AGP unit, N is the fraction of nitrogen in the sample, $\overline{DS}$ is the average degree of substitution per AGP unit, x is the number of nitrogen atoms in the substituent group, and MS is the molar mass of the substituent group. Considering a N of 0.008, x equal to 2, M of 163.982 and MS of 314.34 results in a $\overline{DS}_{AZO}$ per 100 AGP units of 5.1

Take note that this method returns a bulk $\overline{DS}$, in which every OH group is considered viable for substitution. However, considering the intermolecular hydrogen bonds that gives a relative lack of reactivity of the hydroxyl group linked to the C3, and the fact that only the groups on the surface of the crystallites will be available for substitution, difficulty in this type of reaction is to be expected [7]. Indeed the determined $\overline{DS}_{AZO}$ value is around half of what was achieved by Yang et al. [36] in their study of Azo-Cellulose, where the authors using a similar kind of grafting reaction and reaction time, but with a 7 times higher amount of azo-derivative than that used in this work. Nevertheless, the obtained $\overline{DS}$ value for Azo-CNC is on the same order of magnitude of a very similar grafting reaction done by Huang et al. [46] using a fluorescent methylcoumarin functional group.

3.2. Structural and Morphological Properties

Another essential step is the structural and morphological characterization of the novel compound, and to that effect, DRX, AFM and SEM were performed to ascertain whether the Azo-incorporation compromised the CNC nanostructure, alongside the verification of the successful production of the cellulose nanocrystals resultant from the acid hydrolysis reaction of the filter paper with sulfuric acid.

XRD diffraction patterns of the starting material, as well as CNC and Azo-CNC, are represented in Figure 3.3. Observation of the diffractograms clearly shows the characteristic peaks of cellulose Iβ polymorph on all three samples, with the (002) plane peak centered at 22.6º, the (101) peak at 14.7º, and the small (040) contribution at around 33º, maintaining essentially the same pattern across all three of the samples, confirming the stability of the cellulose structure after acid hydrolysis and azo-functionalization [46][47].

Relative crystallinity index (CI) measurements were also taken, using the method of Segal et al. [48] and are represented in Table 3.2. The aforementioned peak height empirical method, involves determining the ratio between the (002) peak height (I_{002}) and the difference between I_{002} and the height of the minimum between the (002) and (101) peaks (the amorphous region) (I_{AM}):

$$CI = \frac{I_{002}-I_{AM}}{I_{002}}$$

As noted by Segal et al., this method is only adequate for quick, comparative measures between samples, and does not provide an accurate gauge for crystallinity, usually even returning values quite above what is accurate for the material [48][49]. However, it is enough, along with the peaks detected in XRD itself, to conclude that the compound preserved its structure. Using an already

high-crystallinity starting point in Whatman filter paper [50], CNC increased its CI, given the removal of amorphous areas during acid hydrolysis. Azo-functionalization maintained the polymorph structure of cellulose I of both preceding materials [49], albeit with a small decrease in crystallinity, due to the amorphous substituents that has been incorporated, as seen in similar reactions in literature, like Lizundia et al.'s work, in which pyrrole grafted to CNC chains had a similar effect of reducing the crystallinity index [51].

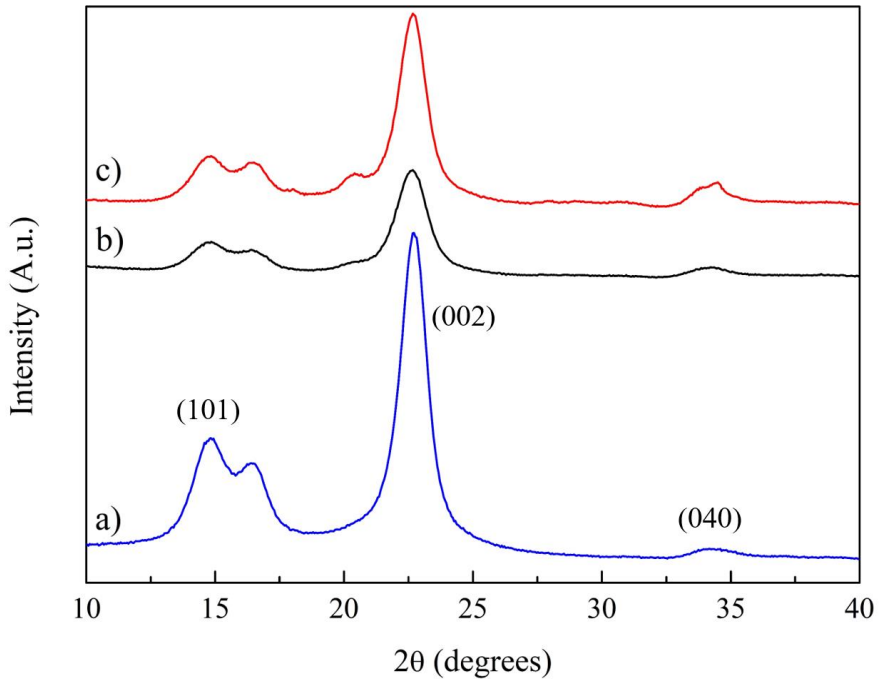

Figure 3.3 – XRD diffraction patterns of a) Filter Paper; b) CNC; c) Azo-CNC.

Table 3.2 – Relative Crystallinity Index measurements through the Segal method

Sample	CI (%)
Filter Paper	91
CNC	93
Azo-CNC	89

AFM and SEM imaging of CNC and Azo-CNC samples was done, confirming that the production of nanoscale materials was successful, with both samples presenting the characteristic elongated rodlike structure, with high aspect ratio[1], as can be seen in Figure 3.4. The average size of CNC and Azo-CNC was also determined from the acquired images, resulting in a measured length of 209±47 nm and 165±39 nm for AFM and SEM respectively, as described in Table 3.3. If we consider the SEM measurements, given their improved resolution over AFM, sizes are in accord with literature of similarly produced CNC, of cotton and filter paper sources [1][45], such as the ones observed through transmission electron microscopy (TEM) by Huang et al. [46].

Observed samples showed some heterogeneity and in the case of AFM measurements, some aggregation that made effective imaging and size measuring difficult. This can be seen in Figure 3.4 and suggests future measurements in AFM may require additional sonication. The intrinsic

flaws of the AFM system also make accurate measurements of nearby, similarly proportioned objects difficult and prone to artifacting, leading to the discrepancy between the AFM and SEM results.

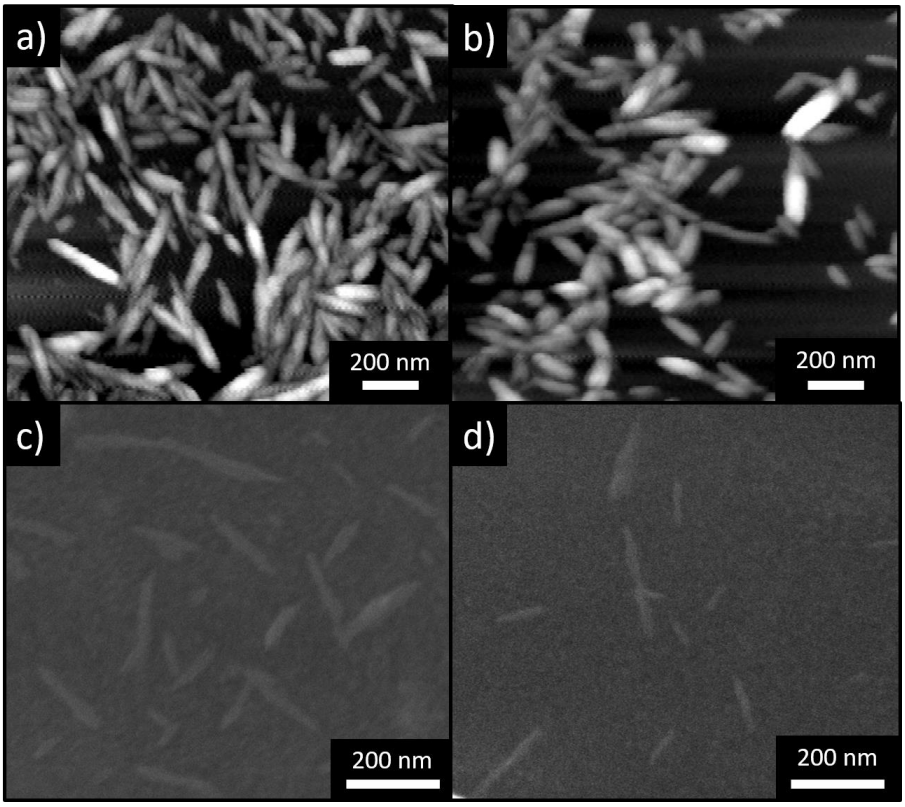

Figure 3.4 – AFM imaging of a) CNC; b) Azo-CNC in height mode and SEM imaging of a) CNC; b) Azo-CNC.

Table 3.3- Dimensions of the produced crystallites

Samples	AFM			SEM		
	Length (nm)	Width (nm)	Aspect Ratio	Length (nm)	Width (nm)	Aspect Ratio
CNC	209±47	46±10	4.6	165±39	17±5	9.4
Azo-CNC	152±38	56±10	2.7	137±40	14±4	9.5

We can now confirm that CNC were successfully prepared and that they remained in the nanoscale after Azo-functionalization (additional images can be found in supplementary information section 6.3).

3.3. Thermal Stability

The resulting TGA curves from filter paper, CNC and Azo-CNC are represented on Figure 3.5. Any weight loss below 100°C can be attributed to moisture evaporation. Following that, the original filter paper sample experiences a rapid decrease of mass between 340°C and 375°C, with

a slower decrease until the end of the test, and keeping in with what is expected for a typical cellulose pyrolysis, this is a first order degradation reaction [52].

The TGA curve of the CNC sample on Figure 3.5 b), shows a sharp decrease of mass at around 160°C and until 245°C, followed by another large decrease at 380°C, followed by slower variation until the conclusion of the test, where still approximately 31% of mass is present. The more gradual decrease of mass seen in CNC, when compared with filter paper, can be associated with the presence of sulfate groups, turning what is normally a one-step pyrolysis process into a two-step reaction, with a lower-temperature phase and a higher-temperature one, similar to Kim et al.'s work on pristine cellulose [52] and what is expected from literature for CNC [45][53][54]. This behaviour can be explained with the first step being cellulose depolymerization, dehydration, and decomposition of the component glycosyl units, followed by the formation of a char, with the second step being the oxidation and breakdown of the char[55]. The presence of sulfate groups has a dehydrating effect on the structure, facilitating the extraction of water from within the structure, and leading to the removal of oxygen, preventing the main means of mass loss during the pyrolysis process, which is the emission of CO and CO_2. This leads to a larger percentage of remaining mass at the end of the test [52].

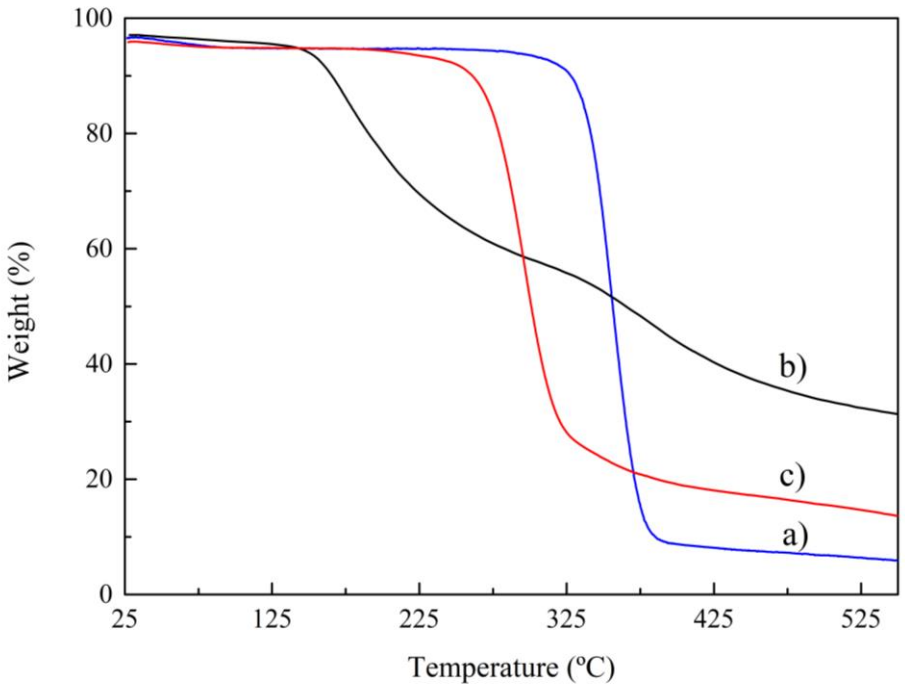

Figure 3.5 – Thermogravimetric curves of a) filter paper; b) CNC; c) Azo-CNC

Unlike unmodified CNC, Azo-CNC possess a curve similar to the starting material, with a sharp decrease of mass at around 270 °C, suggesting that the substituent group provides increased thermal stability to the material. This decrease slows down at 310 °C but continues until the end of the test. This behaviour seems consistent with other functionalized or surface-grafted CNC seen in literature[53][55][56].

Figure 3.6 represents the thermal analysis curves recorded alongside the thermogravimetry. In the case of both filter paper and Azo-CNC, an endothermic peak can be seen at around 350ºC and 300ºC, respectively, representing the sharp mass loss that both those samples experienced at that

temperature. This can be attributed to the to the degradation of the cellulose chains, supporting the hypothesis of a one-step reaction. The CNC sample lacks such a peak, instead having a slightly increased slope, in accordance with its more gradual mass loss in the thermogravimetry test, attributable to a slower and multi-step degradation of the cellulose chains and sulphate derivatives [46][52].

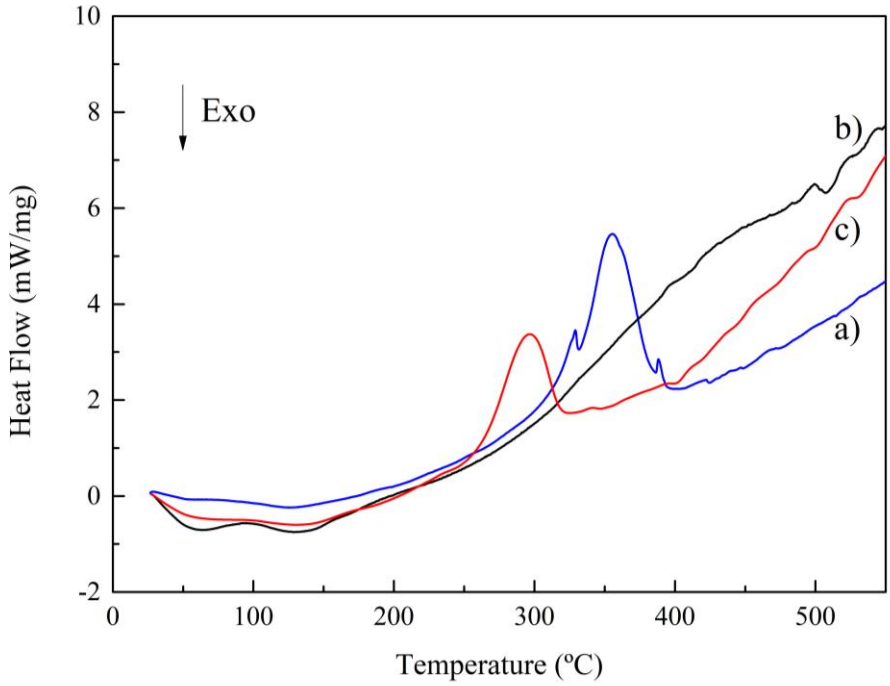

Figure 3.6 – DSC curves of a) Filter paper; b) CNC; c) Azo-CNC.

3.4. Film preparation

Wettability properties of the produced Azo-CNC were to be determined, so therefore, films were produced as described before. A quick examination of all produced films showed them to be quite brittle, in particular all made from Azo-CNC. Removing them from their substrate without additional fractures proved to be a difficult and time-consuming task, with a considerable loss of film, and resulting in somewhat irregular testing sample size and shape. Pristine CNC fared better, but still proved a challenge to prepare, given the reduced uniformity of the produced films.

The CNC film presents a pearly coloration with some hues of yellow and orange and a somewhat metallic shine. The observed hues shift slightly depended on the angle of observation, displaying birefringence. Azo-CNC films, however, displayed a strong, yellow coloration, derived from the azo-benzene derivative used. This coloration possessed a matte appearance on the upward facing surface, in contact with air during drying, and a slight shine on the other, downward facing surface. Images of the prepared films can be seen in
Figure 3.7.

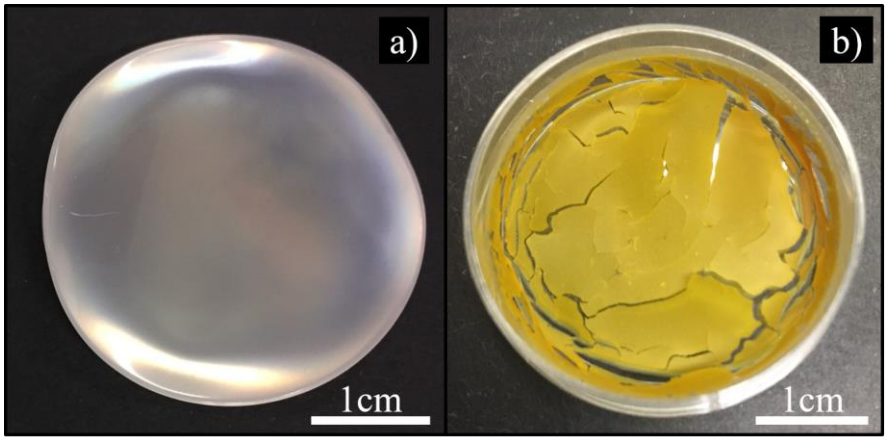

Figure 3.7 – Solvent-cast films of a) CNC; b) Azo-CNC

SEM imaging was done on the cross-section of the prepared film samples, to look into any possible preferential organization in their structure, as seen in Figure 3.8. From Figure 3.8a) it is possible to confirm that cholesteric structures are present in CNC sample, forming pseudo-layers with a cholesteric pitch in average of 372±22 nm, refer to supplementary information, section . This self-ordering structure is characteristic of films produced from aqueous suspension of CNC, which are capable of forming liquid crystal phases, as discussed previously. Reflected light wavelength was estimated using de Vries' theory [57]:

$$\lambda = n \times P \times \sin\theta$$

Where λ is the reflected wavelength, n the mean refractive index for the observed cellulose mesophase, P the pitch of the observed structure and θ the angle of incident light. Therefore, considering a P of 372, a n of 1.54 [58] and a θ of 90º, assuming incident light is normal to the sample surface, the value for the reflected wavelength would be 572 nm (refer to supplementary information section 6.4 for additional images and measured values), resulting in a reflected hue somewhere between yellow and orange (as can be observed on the photographs in Figure 3.7a).

Preliminary wettability tests showed that the CNC and Azo-CNC samples had a tendency to quickly lose structural integrity and redispersed when in contact with water, and so a treatment was required to prevent this. Dankovich et al. [43] developed a thermal treatment during their wettability tests to prevent redispersion, that consisted in heating the prepared films at 105 ºC for 20-30 min. Their method was used in this work, with changes to the experimental conditions, as time and temperature were settled upon through systematic testing. For CNC, the samples required a reduced time, shortening the treatment to 15 min and maintaining the original temperature of 105 ºC. This was done due to early decomposition of the samples. When using these parameters with Azo-CNC the film continued to disintegrate while in contact with water. So, an increase in temperature to 150 ºC was required, while maintaining the 15 min. duration time. This change might be due to the increased thermal resistance of the functionalized compound.

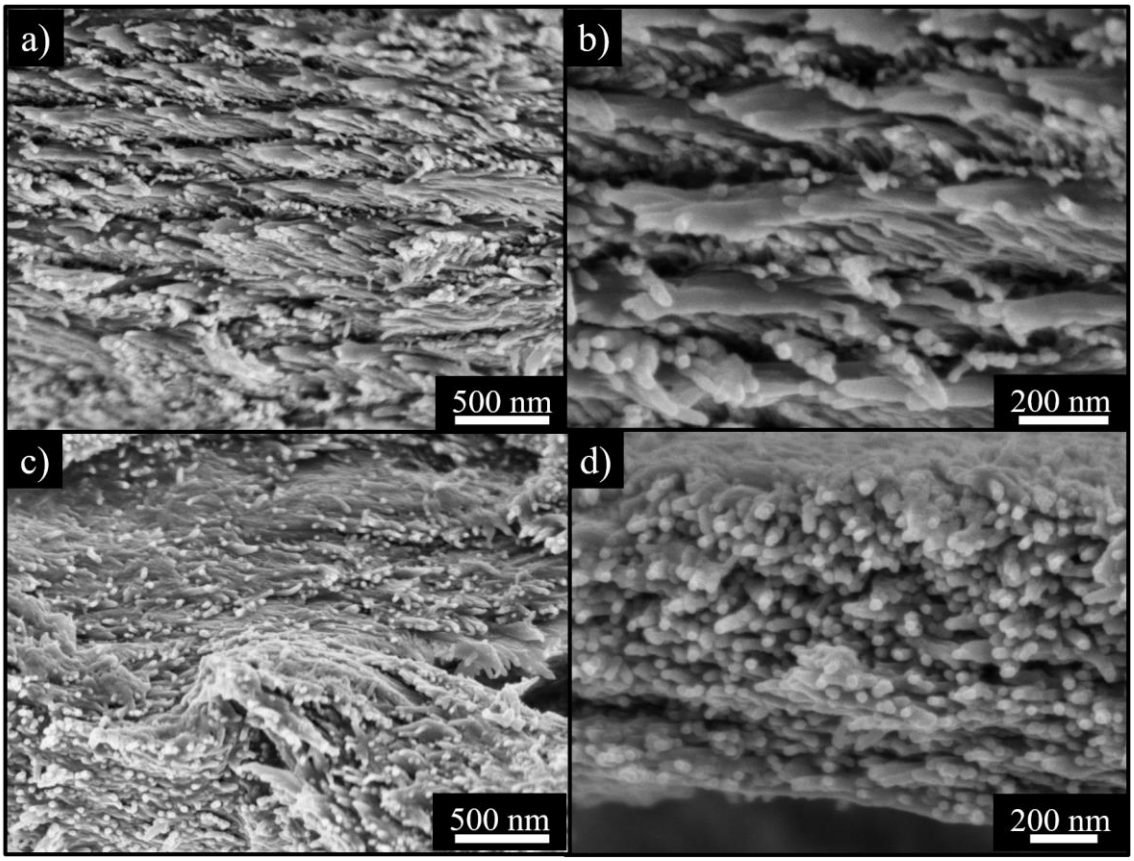

Figure 3.8 – Cross-section SEM images of prepared a), b) CNC films; c), d) Azo-CNC films. Successive pseudo-layers can be observed in the CNC sample, but not in the Azo-CNC film, which is more amorphous.

3.5. Wettability

Two main parameters influence the wettability properties of a given material, which are surface roughness and the chemical composition of that surface. As evidenced by Huang et al. [40] and Pinto et al. [39], the presence of azo moieties affects the wetting properties of azo-cellulose derivatives. Due to this, exploration of the wettability characteristic for CNC and Azo-CNC was done, through sessile drop deposition essays.

Photograph of these sessile drops deposited onto the CNC films surface samples can be seen in Figure 3.9, and static water contact angle measurements were done considering the Young-Laplace method, which is derived from the Young formula for intrinsic contact angle:

$$\cos\theta = \frac{\gamma_{SV}-\gamma_{SL}}{\gamma}$$

In which θ is the Young contact angle, and γ, γ_{SV} and γ_{SL} are the surface tensions for the Liquid/Vapour, Solid/Vapour and Solid/Liquid interfaces [59].

For pristine CNC, at 20-25 ºC and with 30-40% relative humidity, 5 µl drops deposited onto the film substrate, achieved a contact angle value of 35 ± 2º, determined 5 s after drop deposition, demonstrating a hydrophilic behaviour. This value is in good agreement with the values reported in the literature for CNC films of similar source and synthetic conditions [43][60][61].

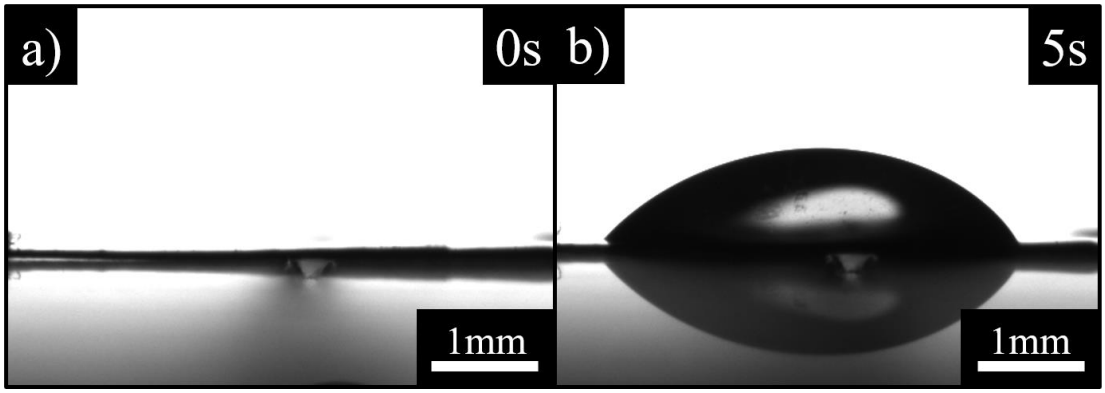

Figure 3.9 – Static contact angle essay consisting of sessile droplet deposit onto pristine CNC films. a) before drop deposition; b) 5 s after drop deposition. Scale taken from the diameter of droplet deposition syringe present in untreated image.

Azo-CNC wettability tests were done under the same conditions as the CNC control samples, but utilizing 2 µl drops, due to film brittleness not allowing the preparation of larger samples. As expected from other similar studies in Azo-substituted cellulose derivatives such as Huang et al.[40] and Pinto et al. [39], there were wettability changes to the material after azo-functionalization.

Figure 3.10 contains photographic examples of droplets deposited onto Azo-CNC films before the moment of drop deposition and just moments after (0.3-2 s). In both examples, the water droplet promptly spread throughout the surface of the film forming a thin, flat layer. The observed response was far greater than reported for other azo-cellulosic derivatives [39][40], presenting what seems to be a superhydrophillic behaviour.

According to Drelich and Chibowski, the term superhydrophilic is applicable to materials who presents a water contact angle lower than 10 º or near-zero, and that according to the Wenzel equation, possess a value of r larger than 1, on which water spreads completely, forming a thin layer[62]:

$$\cos\theta^{*} = \cos\theta \times r$$

Where r is the ratio of the total surface area over the projected area, θ is the Young contact angle, intrinsic to the material, and θ^{*} is the apparent contact angle. Since water completely spreads in contact with the surface of the Azo-CNC samples no contact angle value could be obtained using this optical method. This situation is common and well documented for superhydrophilic surfaces as reviewed by Drelich and Chibowski and Otitoju et al. [62][63].

In addition to complete wetting of the film surface, a mechanical response occurred, in which they displayed remarkable water-responsive bending motion. Images of Azo-CNC films' bending responses are present in Figure 3.11 and Figure 3.12, captured at different times. The sample's initial state, the maximum water-response state, and samples position at the end of the test, when no further motion is observed are depicted. Samples displayed bending, within tens of seconds of water deposition, followed by a slower unbending. A concave curvature was always observable, with the surface on which the water droplet was deposited facing outward. In certain samples, a slow bending response in the opposite direction was also noticed following unbending, which continued for one or two minutes. Bending behaviour was observed independently of what side of the film was chosen for testing, ruling out any interference of surface interactions during the film preparation.

The time to bend, defined as the time required to achieve the maximum bending, was observed as approximately ~ 30 s, however the exact results varied from sample to sample. This can be explained by the heterogeneous nature of the films, and irregular sample size and shape, due to the difficulty in preparing specimens as mentioned above. Proper bending curvature measurements were also not possible due to irregular sample shape and size.

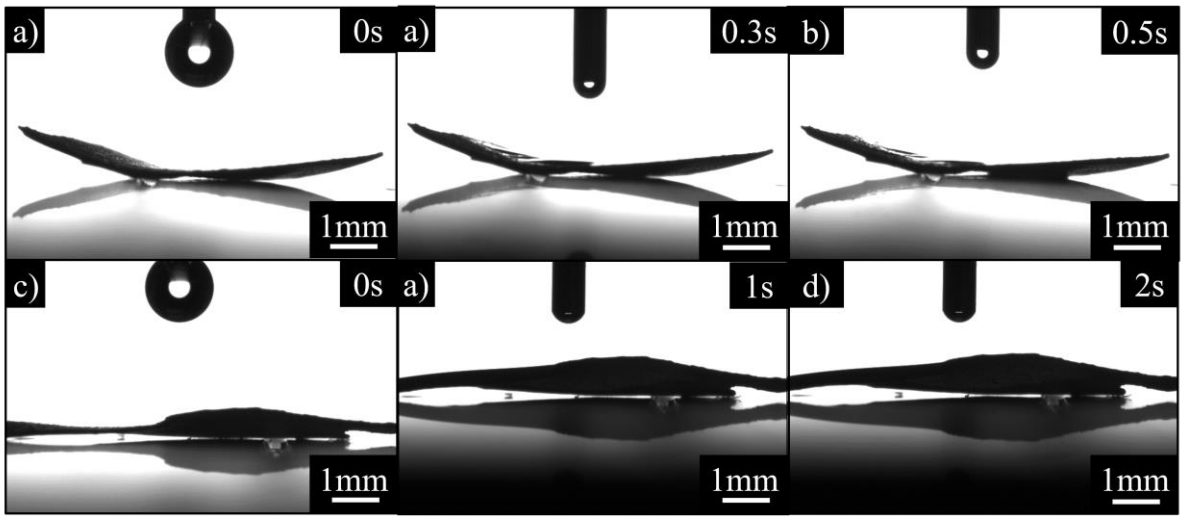

Figure 3.10 – Before and after images of water drop deposition on two Azo-CNC film specimens. a), b) and c), d). Noting the complete wetting of the films

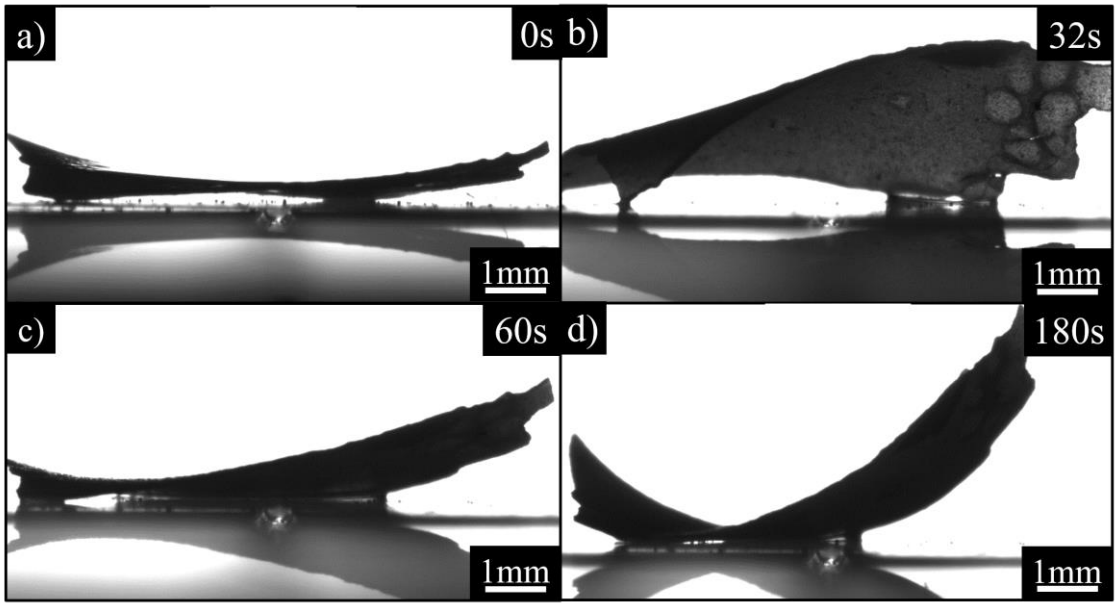

Figure 3.11 – Water-induced response of Azo-CNC film a) before drop deposition; b) at the maximum bending; c) at the point of unbending; d) at the end of sample motion. Of note is the bend in the opposite direction of the initial response present in d).

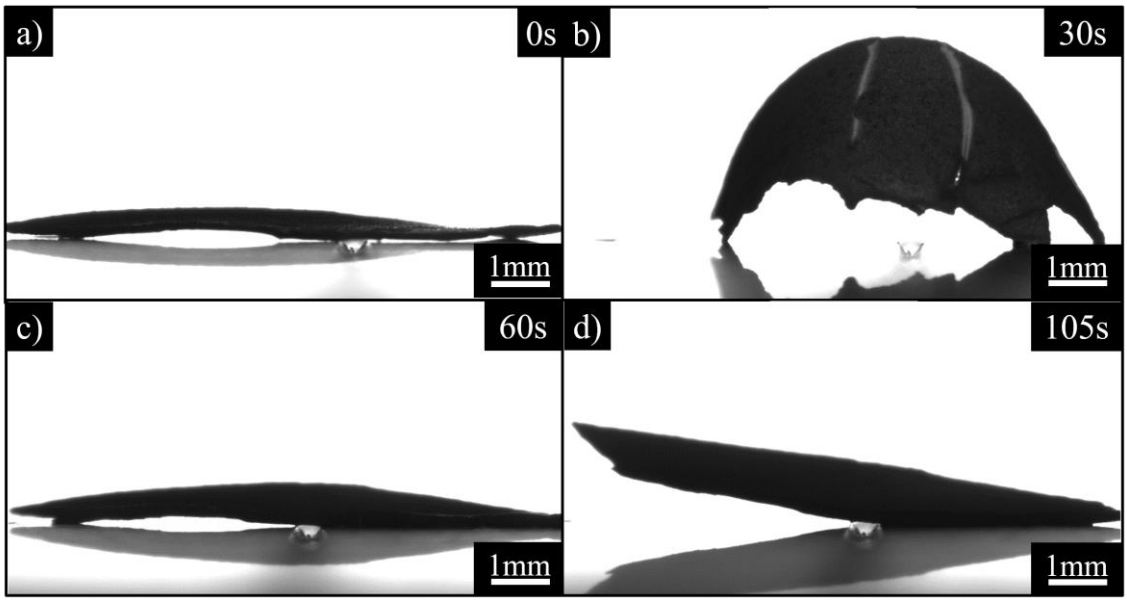

Figure 3.12 – Wettability test-induced response of Azo-CNC film a) before drop deposition; b) at peak bending; c) at the point of unbending d) at the end of sample motion. Note the complete wetting observable in b).

Measurements were also done using a saturated chamber with an atmosphere of 90-95% relative humidity, maintaining temperature and drop sizes. This was done to rule out any possible effects due to the low moisture content in the atmosphere. Additional control samples of pristine CNC in these conditions were also performed with no noticeable change in behaviour, returning a contact angle of 32.5º. Results of essays with Azo-CNC using the saturated chamber continued to follow the behaviour observed in the 30-40% relative humidity atmosphere tests, with the only observable difference being an increase in the unbending time of the samples. Figure 3.13 contain images before deposition and at the moment of peak curvature of Azo-CNC samples tested under saturated atmosphere.

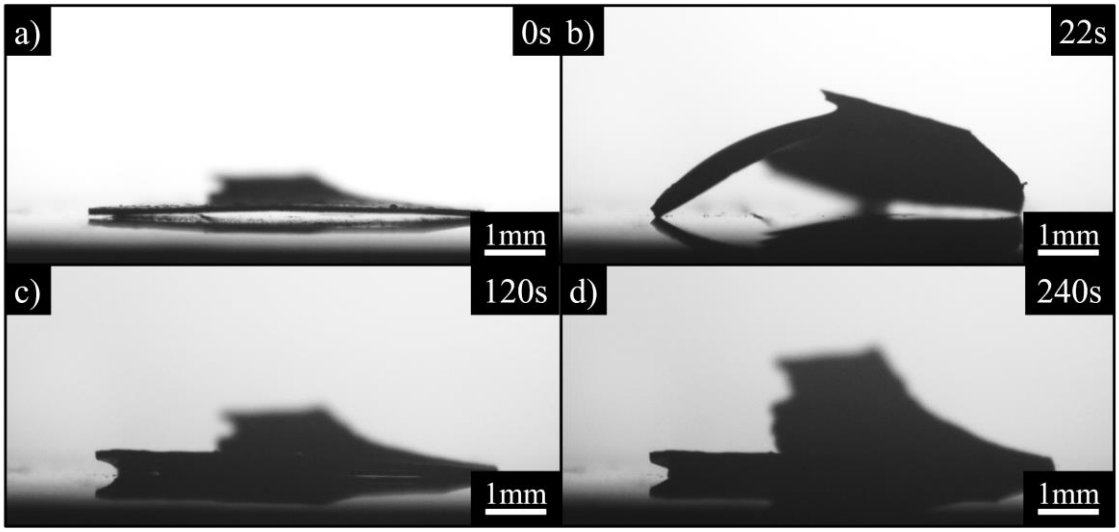

Figure 3.13 – Wettability test of Azo-CNC film under saturated atmosphere a) before drop deposition; b) at peak bending; c) at the point of unbending d) at the end of sample motion.

The water-responsive properties exhibited by our Azo-CNC films are similar to Wang et al.'s study on humidity-responsive MFC films, in which a humidity gradient, through water vapour or

direct hand contact, is established within the film, resulting in a mechanical bending response. They posit that this bending occurs due to swelling of one of the film surfaces when it is exposed to a source of humidity, in a biomimetic reaction akin to that of plant structures, such as pinecones [29]. The various wettability tests performed seem to suggest this that this can also be the case of our system, as schematically represented in Figure 3.14.

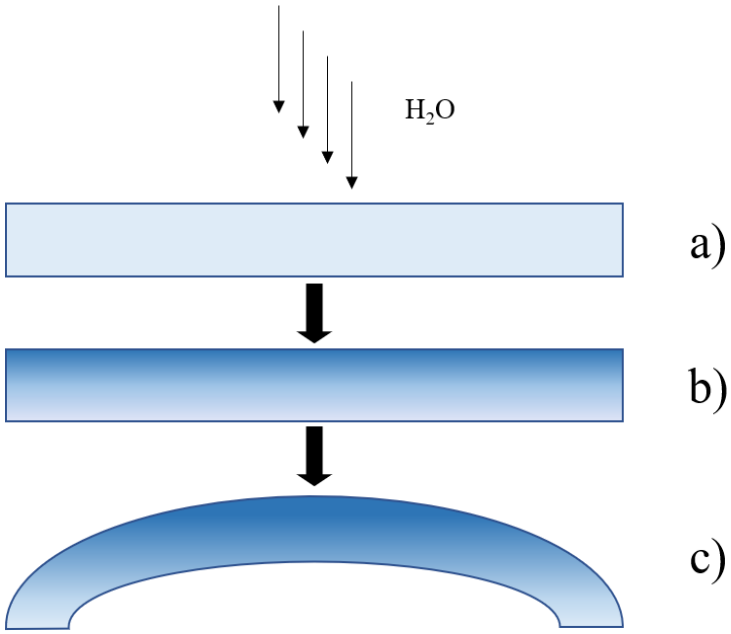

Figure 3.14 – Schematic representation of the response mechanism of Azo-CNC films. a) Contact of water particles with Azo-CNC film surface; b) Formation of a water gradient in the film; c) Swelling of the topmost surface of the film leading to film bending.

Azo-CNC film response to UV radiation was also looked into. Given the superhydrophillic behaviour of the samples, the increase in hydrophilicity from UV exposure described by Pinto et al. and Fernandes et al. [8][39] would be impossible to determine through contact angle measurements. A control test of two samples, pre-UV exposure, was done, followed by exposure for 20 minutes to the above-mentioned UV source and then tested again. The acquired footage was compared, with attention payed to the response time since drop deposition to peak bending, and response times were found to decrease by 6.5 s and 4 s in the two tested samples. An increase in hydrophilicity could be expected to result in faster reaction times due to increasing water intake and making the surface swelling occur faster. Therefore, the water gradient associated with the mechanical response would also occur quicker.

This increase in hydrophilicity would be resultant from the *trans-to-cis*-isomeration of the azo-moieties, activated by the UV exposure. When in the *cis* conformation, the N=N bonds of the azo-moieties become exposed, and hydrogen bonds can easily form between water molecules and the N=N bond. Due to this, the azobenzene derivative is more hydrophilic when in *cis* conformation, compared to the trans isomer [39][40].

Images and reaction times of the film response before and after UV exposure are shown in Figure 3.15.

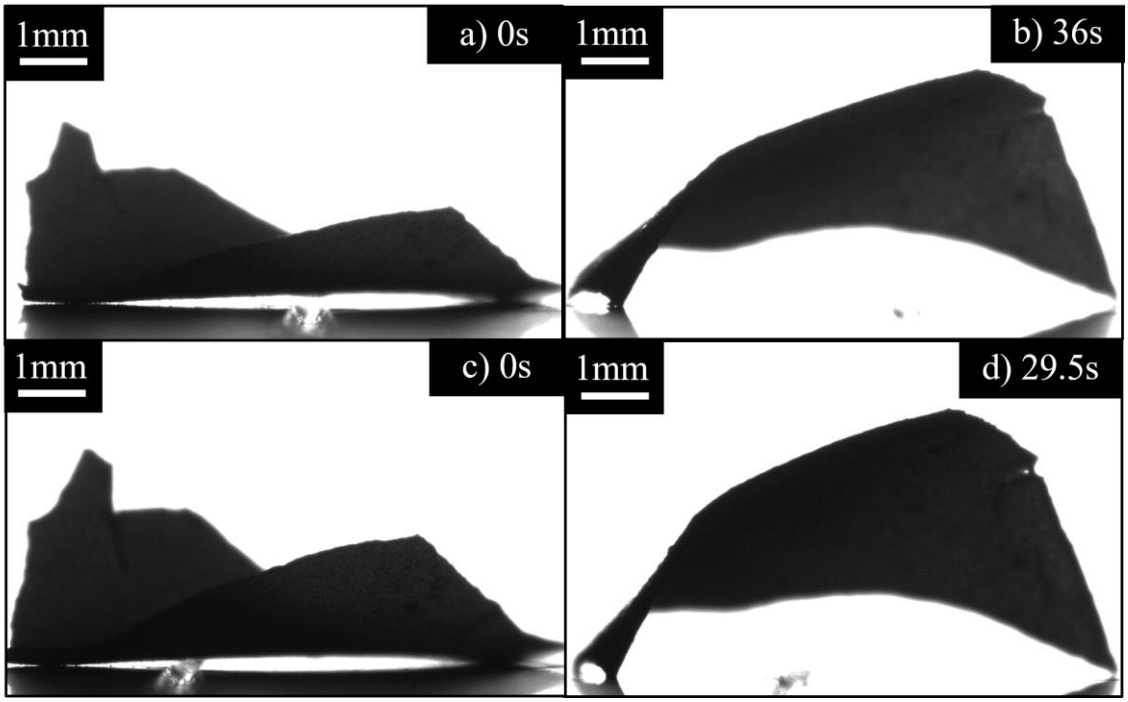

Figure 3.15 – Wettability tests performed on a Azo-CNC sample a),b) before UV exposure; c),d) after 20 min UV exposure. Images on the right represent the peak bending response seen in that test.

4. Conclusion and Future Perspectives

During the development of this project, the main goal was the development of a novel CNC-based compound with stimuli-responsive properties. Towards that goal, CNC suspensions were successfully produced from a cotton filter aid source through acid hydrolysis, with an average length of 209 nm, measure through AFM or 165 nm measured through SEM. The resulting nanocrystals were then used in a catalysed grafting reaction of an azobenzene derivative, giving rise to a new Azo-CNC compound with a remarkable mechanical response to water, with promising indications of tuneability, using UV.

The work was split into steps, including synthesis of CNC, functionalization into Azo-CNC, solvent casting of films, and wettability essays. A battery of chemical, structural and morphological tests were also done on both the produced CNC and the novel Azo-CNC.

Confirmation of successful production of cellulose crystallites in the nanoscale was obtained via SEM and AFM imaging, including the preservation of the native cellulose I structure while increasing crystallinity compared with the starting material, as evidenced by XRD scanning. The functionalization with Azo groups was also confirmed via FTIR and elemental analysis, with the associated $\overline{DS}$ of 0.05 having been determined, with clear indication that the CNC structure and scale were not compromised due to the grafting process. Additionally, the produced CNC were found to be able to form cholesteric liquid crystalline phase while suspended in water, that was imprinted into the solid film giving rise to an structurally coloured film as expected for this type of CNC. Azo-CNC did not seem to organize themselves into such structures, although due to time constraints set on this work, a more complete examination of this capability was not possible, given the time needed for this kind of structural organization.

The azo-moieties grafted onto the CNC granted it improved thermal resistance, increasing the initial decomposition temperature by 110 ºC. While this effect is not unheard for other functionalizing sulphated-CNC, it is very positive and represents a great improvement towards the versatility of application of this polymer.

Films cast from both CNC and Azo-CNC were found to be quite brittle, and in the case of Azo-CNC, the production on a continuous film was not possible. All of this contributed to making a more standardized and systematic approach to the wettability testing very difficult and numerical quantification of the observed mechanical response impossible. However, it was enough to draw solid conclusions for the behaviour of this new material.

During wettability testing, done in order to investigate possible alterations of the hydrophilicity of the new material, it was discovered that the performed functionalization granted Azo-CNC films apparent superhydrophillic properties, with complete surface wetting occurring in a matter of a just few seconds. This keeps in line with the observed wettability trends for other azo-cellulosic derivatives but with a far greater difference, when compared with the hydrophilic character of the CNC. Azo-CNC show an accentuated bending response when put into contact with water droplets during wettability testing, followed by unbending, in an almost completely reversible reaction. When tested under a humidity-saturated atmosphere, they continued to respond, but with comparatively reduced bending, and notably slower unbending, further lending credence to the idea of a gradient-operative response. The Azo-CNC films' remarkable water-response is analogous to the humidity-response displayed by MFC films, in what seems to be a water gradient-driven bending response.

A final wettability test was done in order to investigate the effect of Azo-moiety *trans*-to-*cis*-isomeration on the properties of the prepared films due to UV exposure. Given the

superhydrophillic properties of Azo-CNC, contact angle measurements were not be possible, and so, bending response times were compared. Films that were put through a 20-minute cycle of UV irradiation, at 365 nm, were found to have a quicker response time, with both tested samples respectively reaching peak bending response 6.5 and 4.5 seconds sooner. This could be an indication of further increased hydrophilicity, however further tests should be performed.

Acknowledging the problems faced during the course of this work, much can be done to further study and understand this material and the underlying mechanisms that affect its stimuli-response:

I. Investigate different casting methodology, to facilitate the production of continuous films, to make further testing and quantification easier;
II. Attempt preparation of Azo-CNC suspensions using other solvents, such as THF, ethanol, methanol and formaldehyde, followed by film-casting;
III. Reduce film brittleness, possibly with the incorporation of Azo-CNC in more flexible systems;
IV. Continue testing of the verified UV response, with proper statistical treatment;
V. Synthesis of Azo-CNC with increased Azo amount or reaction times, to produce functionalized material with a higher $\overline{DS}$, to investigate its effects on stimuli-response

The new developed material possesses great potential to be used in new applications, that couples the interesting properties of the cellulose nanocrystal, our starting material, with a remarkable mechanical response and superhydrophillic properties, verified despite low azo-substituent incorporation. Promising applications could be the inclusion of this polymer as filler in composite systems, generating the so-called “smart materials”. One can also foresee the application of Azo-CNC in stimuli-responsive memory shape polymer composites, specifically water-active polymer composites, where the superhydrophillic properties of Azo-CNC and potentially tuneable response is of most importance.

5. References

[1] D. Klemm *et al.*, "Nanocelluloses: A New Family of Nature-Based Materials," *Angew. Chemie Int. Ed.*, vol. 50, no. 24, pp. 5438–5466, 2011.

[2] J. S. Park, T. Kim, and W. S. Kim, "Conductive Cellulose Composites with Low Percolation Threshold for 3D Printed Electronics," *Sci. Rep.*, vol. 7, 2016, pp. 1–10, 2017.

[3] M. R. Wilson, D. S. Jones, and G. P. Andrews, "The development of sustained release drug delivery platforms using melt-extruded cellulose-based polymer blends," *J. Pharm. Pharmacol.*, vol. 69, pp. 32–42, 2017.

[4] "VDP - Facts about Paper," 2017. [Online]. Available: https://www.vdp-online.de. [Accessed: 20-Nov-2017].

[5] W. Y. Hamad, "Assembly and Structure in Native Cellulosic Fibers," in *Cellulose nanocrystals : properties, production, and applications*, C. V. Stevens, Ed. Chichester, West Sussex: John Wiley & Sons Ltd, ch. 2, pp. 16–32, 2017.

[6] Y. Habibi, L. A. Lucia, and O. J. Rojas, "Cellulose Nanocrystals : Chemistry , Self-Assembly , and Applications," *Chem. Rev.*, vol. 110, pp. 3479–3500, 2010.

[7] S. Eyley and W. Thielemans, "Surface modification of cellulose nanocrystals," *Nanoscale*, vol. 6, pp. 7764–7779, 2014.

[8] S. N. Fernandes *et al.*, "Cellulose-based nanostructures for photoresponsive surfaces," *Cellulose*, vol. 23, pp. 465–476, 2016.

[9] R. H. Atalla and A. Isogai, "Recent Developments in Spectroscopic and Chemical Characterization of Cellulose Rajai," in *Polysaccharides: Structural Diversity and Functional Versatility*, S. Dumitriu, Ed. Quebec, Canada: Marcel Dekker, ch. 5, pp. 123–158, 1998.

[10] M. H. H. Godinho, D. G. G. Gray, and P. Pieranski, "Revisiting (hydroxypropyl) cellulose (HPC)/water liquid crystalline system," *Liq. Cryst.*, vol. 44, no. 12–13, pp. 2108–2120, 2017.

[11] B. Ghanbarzadeh, H. Almasi, and A. A. Entezami, "Improving the barrier and mechanical properties of corn starch-based edible films : Effect of citric acid and carboxymethyl cellulose," *Ind. Crop. Prod.*, vol. 33, pp. 229–235, 2011.

[12] K. Missoum, M. Belgacem, and J. Bras, "Nanofibrillated Cellulose Surface Modification: A Review," *Materials (Basel).*, vol. 6, pp. 1745–1766, 2013.

[13] M. Hasani, E. D. Cranston, G. Westman, and D. G. Gray, "Cationic surface functionalization of cellulose nanocrystals," *Soft Matter*, vol. 4, pp. 2238–2244, 2008.

[14] B. G. Rånby, A. Banderet, and L. G. Sillén, "Aqueous Colloidal Solutions of Cellulose Micelles.," *Acta Chem. Scand.*, vol. 3, pp. 649–650, 1949.

[15] H. M. Ng, L. T. Sin, S. T. Bee, T. T. Tee, and A. R. Rahmat, "Review of Nanocellulose Polymer Composite Characteristics and Challenges," *Polym. - Plast. Technol. Eng.*, vol. 56, pp. 687–731, 2017.

[16] S. Beck-Candanedo, M. Roman, and D. G. Gray, "Effect of reaction conditions on the properties and behavior of wood cellulose nanocrystal suspensions," *Biomacromolecules*, vol. 6, pp. 1048–1054, 2005.

[17] W. Y. Hamad, "Hydrolytic Extraction of Cellulose Nanocrystals," in *Cellulose nanocrystals : properties, production, and applications*, C. V. Stevens, Ed. Chichester, West Sussex: John Wiley & Sons Ltd, ch. 3, 2017, pp. 33–62.

[18] S. N. Fernandes *et al.*, "Mind the Microgap in Iridescent Cellulose Nanocrystal Films," *Adv. Mater.*, vol. 29, 2017, 1603560.

[19] J. Revol, H. Bradford, J. Giasson, R. H. Marchessault, and D. G. Gray, "Helicoidal self-ordering of cellulose microfibrils in aqueous suspension," *Int. J. Biol. Macromol.*, vol. 14, pp. 170–172, 1992.

[20] W. Y. Hamad, "Properties of Cellulose Nanocrystals," in *Cellulose nanocrystals : properties, production, and applications*, C. V. Stevens, Ed. ,Chichester, West Sussex,

England: John Wiley & Sons Ltd, ch. 4, pp. 65–134, 2017.
[21] M. Chaichi, M. Hashemi, F. Badii, and A. Mohammadi, “Preparation and characterization of a novel bionanocomposite edible film based on pectin and crystalline nanocellulose,” *Carbohydr. Polym.*, vol. 157, pp. 167–175, 2017.
[22] A. Herreros-López *et al.*, “Nanocrystalline cellulose-fullerene: Novel conjugates,” *Carbohydr. Polym.*, vol. 164, pp. 92–101, 2017.
[23] P. Theato, B. S. Sumerlin, R. K. O’Reilly, and T. H. Epps, III, “Stimuli responsive materials,” *Chem. Soc. Rev.*, vol. 42, p. 7055, 2013.
[24] G. Zhang *et al.*, “Novel Piezoelectric Paper-Based Flexible Nanogenerators Composed of BaTiO 3 Nanoparticles and Bacterial Cellulose,” *Adv. Sci.*, vol. 3, 2016, 1500257.
[25] N. Li, W. Chen, G. Chen, and J. Tian, “Rapid shape memory TEMPO-oxidized cellulose nanofibers/polyacrylamide/gelatin hydrogels with enhanced mechanical strength,” *Carbohydr. Polym.*, vol. 171, pp. 77–84, 2017.
[26] C. Shao, M. Wang, H. Chang, F. Xu, and J. Yang, “A Self-Healing Cellulose Nanocrystal-Poly(ethylene glycol) Nanocomposite Hydrogel via Diels-Alder Click Reaction,” *ACS Sustain. Chem. Eng.*, vol. 5, pp. 6167–6174, 2017.
[27] X. Qiu and S. Hu, “‘Smart’ materials based on cellulose: A review of the preparations, properties, and applications,” *Materials (Basel).*, vol. 6, pp. 738–781, 2013.
[28] Y. Geng, P. L. Almeida, S. N. Fernandes, C. Cheng, P. Palffy-Muhoray, and M. H. Godinho, “A cellulose liquid crystal motor: a steam engine of the second kind,” *Sci. Rep.*, vol. 3, 2013, 1028.
[29] M. Wang, X. Tian, R. H. A. Ras, and O. Ikkala, “Sensitive Humidity-Driven Reversible and Bidirectional Bending of Nanocellulose Thin Films as Bio-Inspired Actuation,” *Adv. Mater. Interfaces*, vol. 2, pp. 1–7, 2015.
[30] Y. Wei, Q. Tang, C. Gong, and M. H.-W. Lam, “Review of the recent progress in photoresponsive molecularly imprinted polymers containing azobenzene chromophores,” *Anal. Chim. Acta*, vol. 900, pp. 10–20, 2015.
[31] J. García-Amorós and D. Velasco, “Recent advances towards azobenzene-based light-driven real-time information-transmitting materials,” *Beilstein J. Org. Chem.*, vol. 8, pp. 1003–1017, 2012.
[32] K. Ichimura, S. K. Oh, and M. Nakagawa, “Light-driven motion of liquids on a photoresponsive surface,” *Science (80-.).*, vol. 288, pp. 1624–1626, 2001.
[33] H. Yu and T. Ikeda, “Photocontrollable liquid-crystalline actuators,” *Adv. Mater.*, vol. 23, pp. 2149–2180, 2011.
[34] T. Ikeda, M. Nakano, Y. Yu, O. Tsutsumi, and A. Kanazawa, “Anisotropic bending and unbending behavior of azobenzene liquid-crystalline gels by light exposure,” *Adv. Mater.*, vol. 15, pp. 201–204, 2003.
[35] G. Koçer *et al.*, “Light-Responsive Hierarchically Structured Liquid Crystal Polymer Networks for Harnessing Cell Adhesion and Migration,” *Adv. Mater.*, vol. 29, pp. 1–8, 2017.
[36] S. Yang, M. M. Jacob, L. Li, A. L. Cholli, J. Kumar, and S. K. Tripathy, “Synthesis and characterization of novel azobezene-modified polymers: Azocellulose,” *Macromolecules*, vol. 34, pp. 9193–9196, 2001.
[37] X. Hu, P. J. Zheng, X. Y. Zhao, L. Li, K. C. Tam, and L. H. Gan, “Preparation, characterization and novel photoregulated rheological properties of azobenzene functionalized cellulose derivatives and their α-CD complexes,” *Polymer (Guildf).*, vol. 45, pp. 6219–6225, 2004.
[38] M. Lizu, M. R. Lutfor, N. L. Surugau, S. E. How, and S. E. Arshad, “Synthesis and Characterization of Ethyl Cellulose–Based Liquid Crystals Containing Azobenzene Chromophores,” *Mol. Cryst. Liq. Cryst.*, vol. 528, pp. 64–73, 2010.
[39] L. F. V. Pinto *et al.*, “Cellulose-based liquid crystalline photoresponsive films with tunable surface wettability,” *Langmuir*, vol. 27, pp. 6330–6337, 2011.

[40] Y. Huang, H. Kang, G. Li, C. Wang, Y. Huang, and R. Liu, “Synthesis and photosensitivity of azobenzene functionalized hydroxypropylcellulose,” *RSC Adv.*, vol. 3, 2013, 15909.
[41] X. M. Dong, T. Kimura, J.-F. Revol, and D. G. Gray, “Effects of Ionic Strength on the Isotropic−Chiral Nematic Phase Transition of Suspensions of Cellulose Crystallites,” *Langmuir*, vol. 12, pp. 2076–2082, Jan. 1996.
[42] S. Beck, M. Méthot, and J. Bouchard, “General procedure for determining cellulose nanocrystal sulfate half-ester content by conductometric titration,” *Cellulose*, vol. 22, pp. 101–116, 2015.
[43] T. A. Dankovich and D. G. Gray, “Contact Angle Measurements on Smooth Nanocrystalline Cellulose (I) Thin Films,” *J. Adhes. Sci. Technol.*, vol. 25, pp. 699–708, 2011.
[44] W. Y. Hamad and T. Q. Hu, “Structure-process-yield interrelations in nanocrystalline cellulose extraction,” *Can. J. Chem. Eng.*, vol. 88, pp. 392–402, 2010.
[45] D. Gaspar *et al.*, “Nanocrystalline cellulose applied simultaneously as the gate dielectric and the substrate in flexible field effect transistors,” *Nanotechnology*, vol. 25, Mar. 2014, 094008.
[46] J. L. Huang, C. J. Li, and D. G. Gray, “Cellulose nanocrystals incorporating fluorescent methylcoumarin groups,” *ACS Sustain. Chem. Eng.*, vol. 1, pp. 1160–1164, 2013.
[47] M. Wada, T. Okano, and J. Sugiyama, “Synchrotron-radiated X-ray and neutron diffraction study of native cellulose,” *Cellulose*, vol. 4, pp. 221–232, 1997.
[48] L. Segal, J. J. Creely, A. E. Martin, and C. M. Conrad, “An Empirical Method for Estimating the Degree of Crystallinity of Native Cellulose Using the X-Ray Diffractometer,” *Text. Res. J.*, vol. 29, pp. 786–794, 1959.
[49] S. Park, J. O. Baker, M. E. Himmel, P. A. Parilla, and D. K. Johnson, “Cellulose crystallinity index: measurement techniques and their impact on interpreting cellulase performance,” *Biotechnol. Biofuels*, vol. 3, p.10, 2010.
[50] A. C. W. Leung *et al.*, “Characteristics and properties of carboxylated cellulose nanocrystals prepared from a novel one-step procedure,” *Small*, vol. 7, pp. 302–305, 2011.
[51] E. Lizundia, T.-D. Nguyen, J. L. Vilas, W. Y. Hamad, and M. J. MacLachlan, “Chiroptical, morphological and conducting properties of chiral nematic mesoporous cellulose/polypyrrole composite films,” *J. Mater. Chem. A*, vol. 5, pp. 19184–19194, 2017.
[52] D. Y. Kim, Y. Nishiyama, M. Wada, and S. Kuga, “High-yield carbonization of cellulose by sulfuric acid impregnation,” *Cellulose*, vol. 8, pp. 29–33, 2001.
[53] L. Petersson, I. Kvien, and K. Oksman, “Structure and thermal properties of poly(lactic acid)/cellulose whiskers nanocomposite materials,” *Compos. Sci. Technol.*, vol. 67, pp. 2535–2544, 2007.
[54] N. F. Vasconcelos *et al.*, “Bacterial cellulose nanocrystals produced under different hydrolysis conditions: Properties and morphological features,” *Carbohydr. Polym.*, vol. 155, pp. 425–431, 2017.
[55] X. Cao, Y. Habibi, and L. A. Lucia, “One-pot polymerization, surface grafting, and processing of waterborne polyurethane-cellulose nanocrystal nanocomposites,” *J. Mater. Chem.*, vol. 19, p. 7137–7145, 2009.
[56] M. Pracella, M. M. U. Haque, and D. Puglia, “Morphology and properties tuning of PLA/cellulose nanocrystals bio-nanocomposites by means of reactive functionalization and blending with PVAc,” *Polym. (United Kingdom)*, vol. 55, pp. 3720–3728, 2014.
[57] H. de Vries, “Rotatory power and other optical properties of certain liquid crystals,” *Acta Crystallogr.*, vol. 4, pp. 219–226, 1951.
[58] R. J. Moon, A. Martini, J. Nairn, J. Simonsen, and J. Youngblood, *Cellulose nanomaterials review: structure, properties and nanocomposites*, vol. 40, pp. 3941-3994, 2011.

[59] G. Whyman, E. Bormashenko, and T. Stein, “The rigorous derivation of Young, Cassie-Baxter and Wenzel equations and the analysis of the contact angle hysteresis phenomenon,” *Chem. Phys. Lett.*, vol. 450, pp. 355–359, 2008.
[60] L. Valentini, M. Cardinali, E. Fortunati, L. Torre, and J. M. Kenny, “A novel method to prepare conductive nanocrystalline cellulose/graphene oxide composite films,” *Mater. Lett.*, vol. 105, pp. 4–7, 2013.
[61] E. D. Cranston, D. G. Gray, and M. W. Rutland, “Direct surface force measurements of polyelectrolyte multilayer films containing nanocrystalline cellulose,” *Langmuir*, vol. 26, pp. 17190–17197, 2010.
[62] J. Drelich and E. Chibowski, “Superhydrophilic and Superwetting Surfaces: Definition and Mechanisms of Control,” *Langmuir*, vol. 26, pp. 18621–18623, Dec. 2010.
[63] T. A. Otitoju, A. L. Ahmad, and B. S. Ooi, “Superhydrophilic (superwetting) surfaces: A review on fabrication and application,” *J. Ind. Eng. Chem.*, vol. 47, pp. 19–40, 2017.

6. Supplementary Information

6.1. Materials and Methods

Elemental analysis was performed on Requimte Laboratory (within FCT-UNL), with a Thermo Finnigan-CE Instruments Flash EA 1112 CHNS series model elemental analyser.

Scanning calorimetry with thermogravimetric analysis (DSC-TGA) was conducted, using samples of approximately 6 mg, with a Netzsch 449 F3 Jupiter® simultaneous thermal analyser, at a heating rate of 10 ºC/min from 25ºC to 550 ºC, in an inert Nitrogen atmosphere.

General microscopy observation and cross-polarized imaging (POM) was done using an Olympus BX21 optical microscope and an associated Olympus DP73 CCD camera and Olympus KL2500 LCD cold light source, with the Olympus Stream Basic v.1.9 image acquisition software.

General photography was done with an iPhone 6, equipped with an 8 MP iSight camera.

X-ray diffraction (XRD) spectra of samples were acquired with a PANalytical X'pert PRO model diffractometer, with Bragg-Brentano geometry with Cu K (1.54 Å) radiation at 45 kV and 40 mA. The XRD patterns were collected with a scanning step of 0.0334º over the angular 2θ range of 10º–40º, with a total acquisition time of 4 min.

Attenuated total reflectance Fourier-transformed infrared (ATR-FTIR) spectra were collected using a Thermo-Nicolet 6700 spectrometer with a Smart iTR sampling accessory. Measurements were done at 20 ºC, within the frequency range of 550 cm-1 to 4000 cm-1, at an incident angle of 45º and with a resolution of 4 cm^{-1}.

6.2 General microscopy and photography

Cross-polarized optical microscopy was done on fibres of the starting filter paper, in order to determine average fibre size. The utilized image is presented in Figure 6.1.

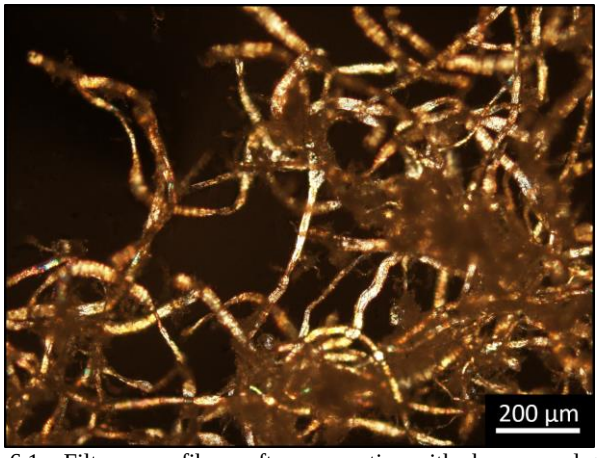

Figure 6.1 – Filter paper fibres, after preparation with chopper and grinder.

A sample image was taken of a prepared CNC suspension exhibiting clear birefringence and is presented in Figure 6.2.

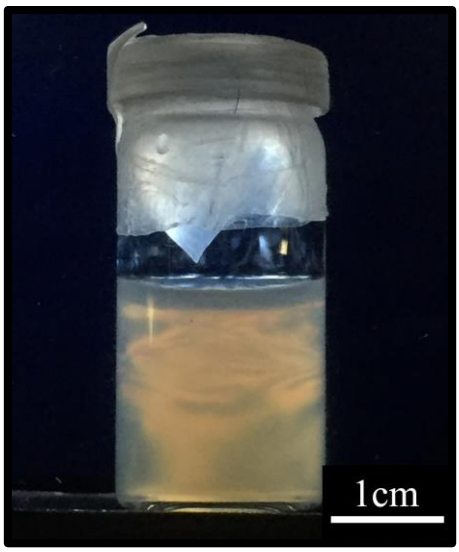

Figure 6.2 – Photographed of a aqueous CNC suspension 4 % (w/w) obtained between crossed polarizers demonstrating clear birefringence.

6.3 CNC aspect ratio

Using captured AFM and SEM images and both Gwyddion and ImageJ software, average length and width measurements were done to determine CNC and Azo-CNC aspect ratio. The used SEM images are Figure 6.3 and Figure 6. 4 for Azo-CNC and Figure 6.5 and Figure 6.6 for CNC. The used AFM images are Figure 6. 7 and Figure 6. 8 for Azo-CNC and Figure 6. 9 for CNC. Measurements can be found in Table 6. 1 AFM and Table 6.2 for SEM.

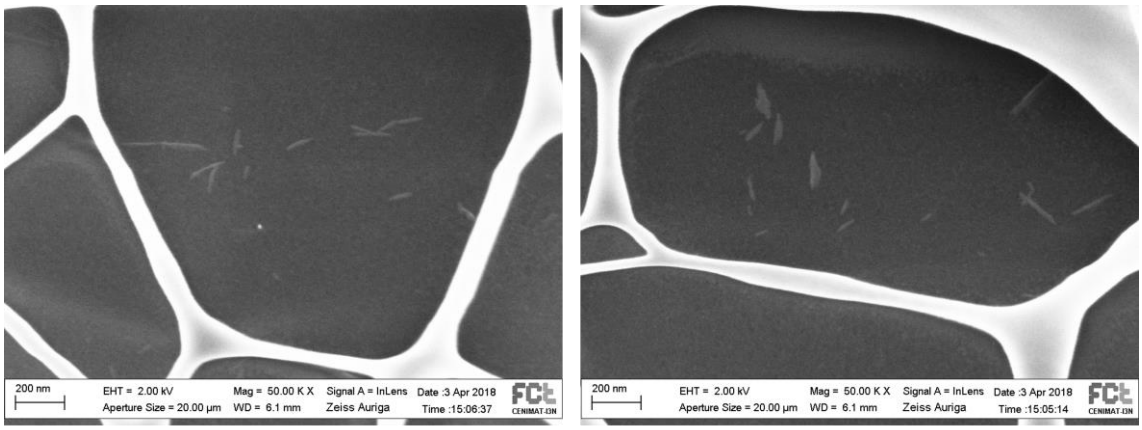

Figure 6.3 – SEM imaging of Azo-CNC used for aspect ratio determination.

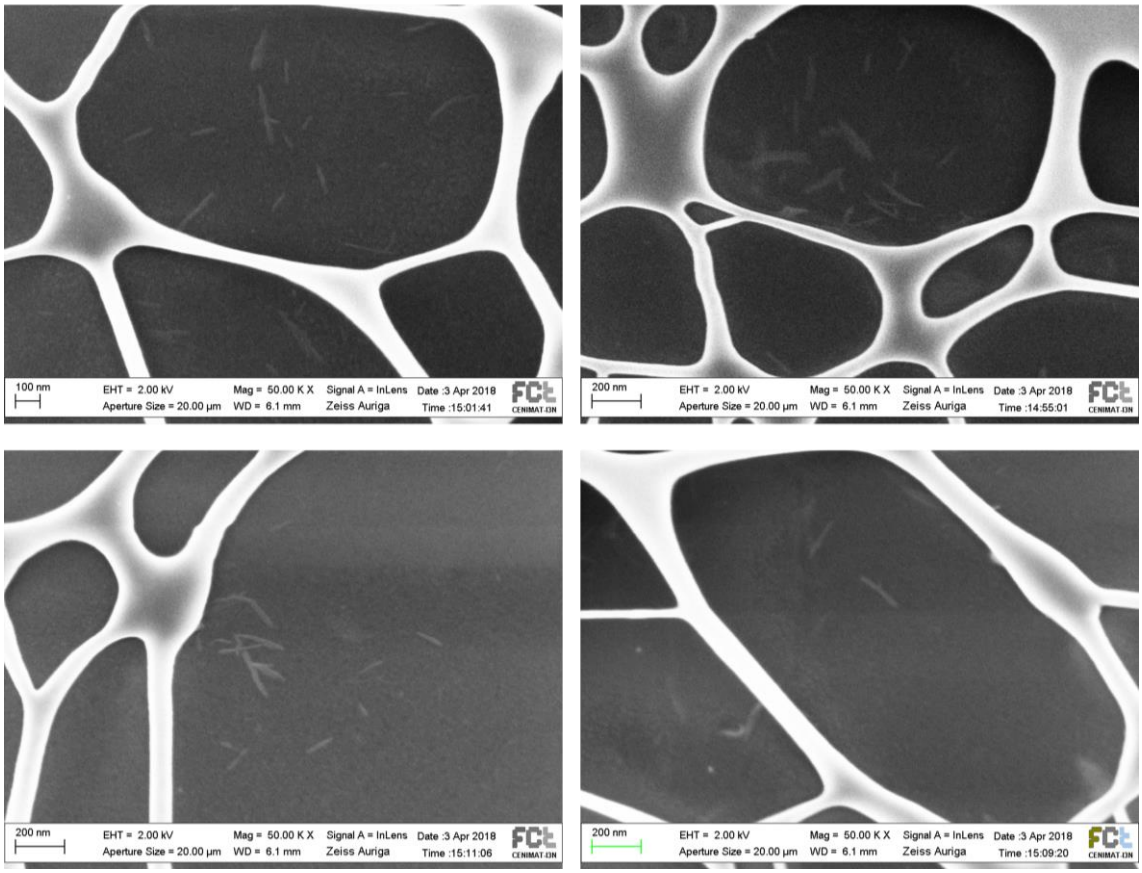

Figure 6. 4 – SEM imaging of Azo-CNC used for aspect ratio determination.

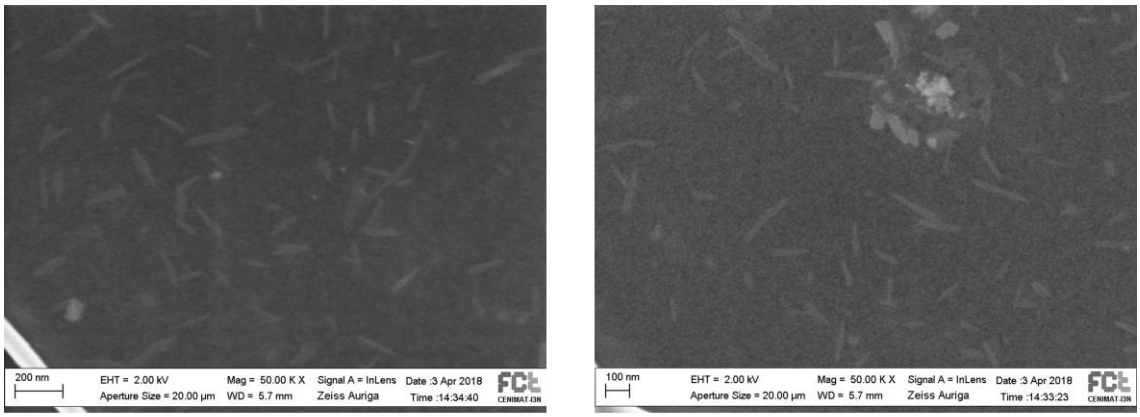

Figure 6.5 – SEM imaging of CNC used for aspect ratio determination.

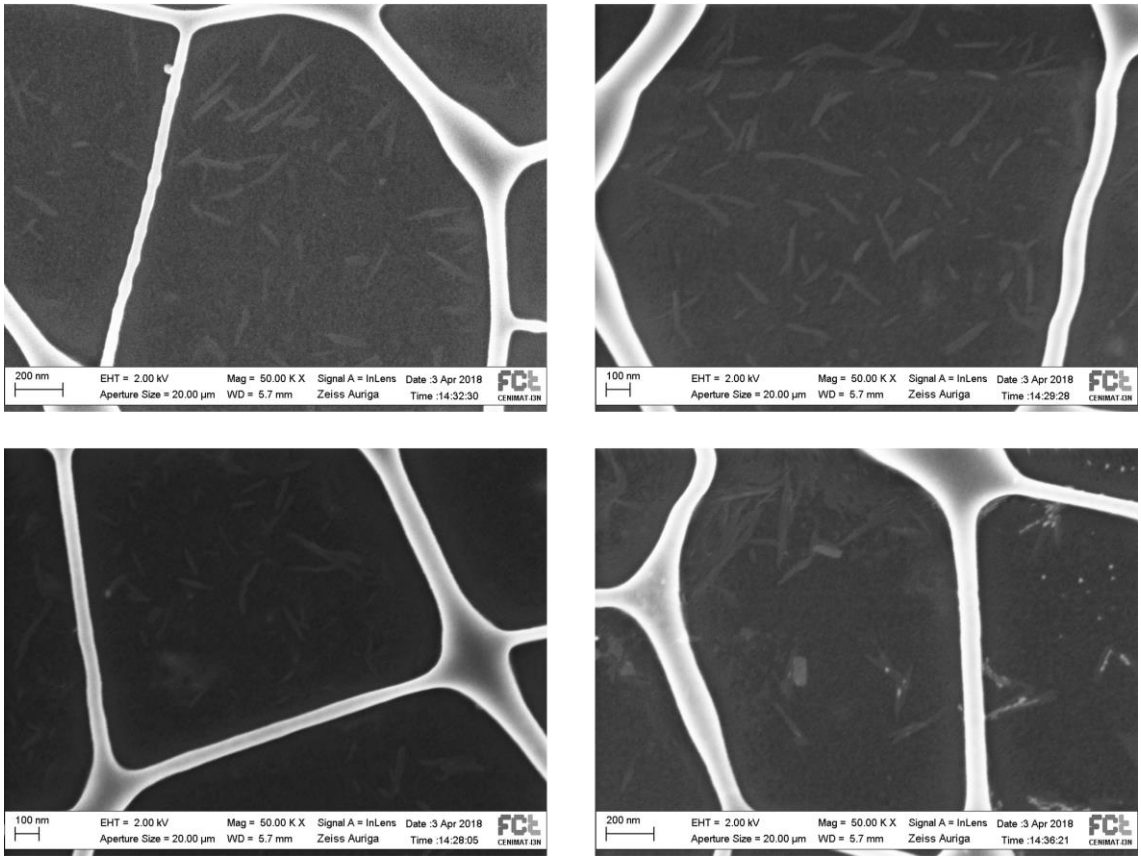

Figure 6.6 – SEM imaging of CNC used for aspect ratio determination.

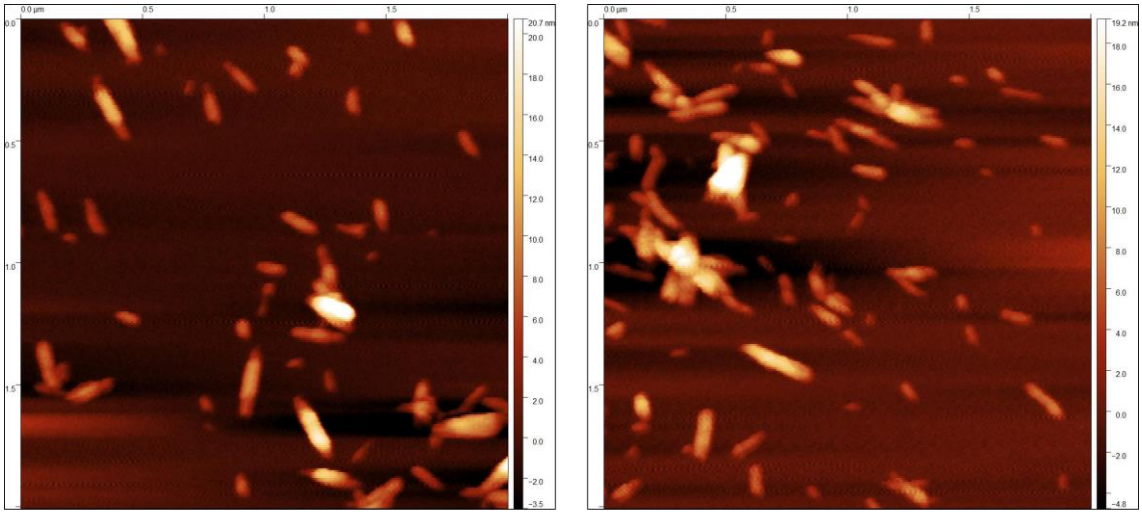

Figure 6. 7 – AFM imaging of Azo-CNC used for aspect ratio determination.

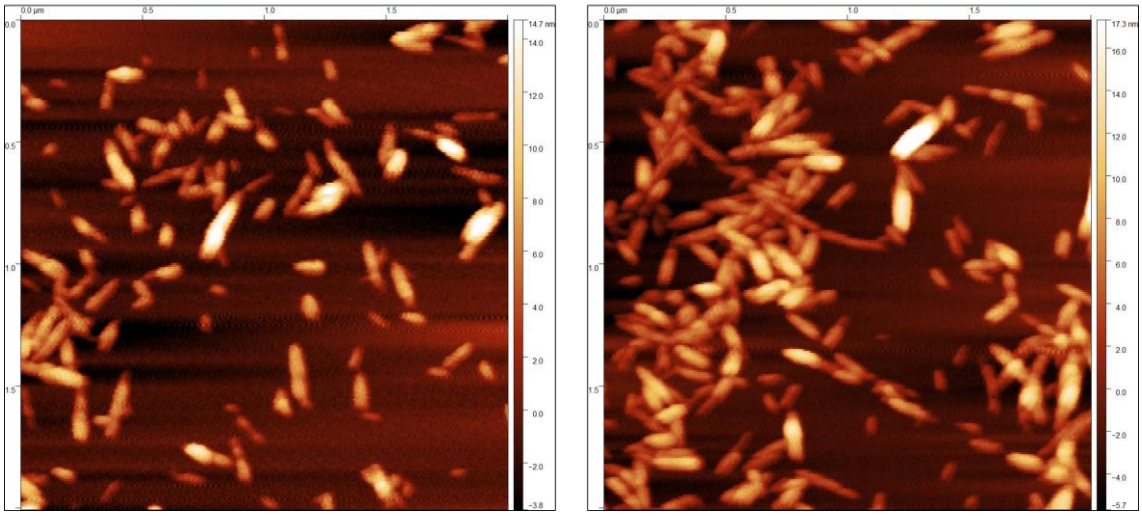

Figure 6. 8 – AFM imaging of Azo-CNC used for aspect ratio determination.

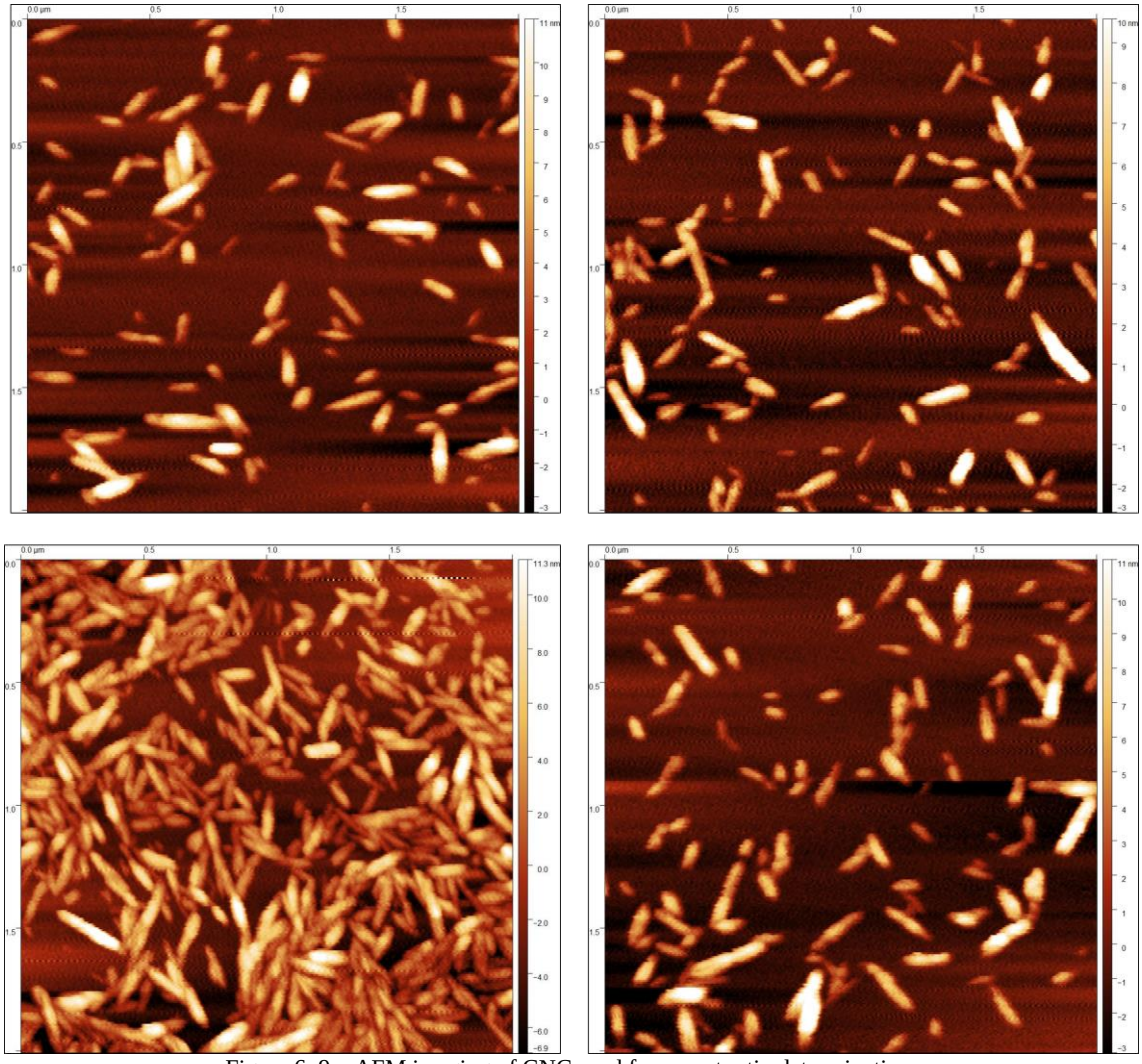

Figure 6. 9 – AFM imaging of CNC used for aspect ratio determination.

Table 6. 1 – Measurements done for aspect ratio determination with AFM images

AFM							
CNC				Azo-CNC			
Length (nm)		Width (nm)		Length (nm)		Width (nm)	
243	209	48	38	243	145	56	45
195	173	56	51	142	134	46	52
200	215	50	27	137	161	43	64
220	167	33	23	150	112	54	59
224	193	43	31	173	140	42	55
183	251	47	27	133	261	64	68
165	245	50	68	119	126	50	66
194	315	37	52	140	159	49	64
173	273	43	49	100	152	55	55
301	252	32	66	152	140	58	51
228	235	41	52	130	130	56	39
139	200	41	51	172	180	53	45
145	179	37	42	100	116	66	50
194	162	39	45	184	272	64	65
177	222	52	61	133	162	46	54
209	313	53	48	201	268	60	88
149	216	44	61	135	162	70	76
142	198	52	35	187	147	65	59
208	233	55	61	126	174	64	73
158	203	42	58	158	161	37	57
173	282	51	52	133	198	48	61
185	210	45	42	117	140	37	62
272	211	42	43	137	155	62	60
197	170	56	38	140	135	57	53
398	167	49	45	151	104	49	64
181	194	44	66				
231	156	38	50				
246	159	54	39				
218	---------	31	34				

Table 6.2 – Measurements done for aspect ratio determination with SEM images

SEM							
AZO				CNC			
Length (nm)		Width (nm)		Length (nm)		Width (nm)	
173	65	20	11	103	108	21	6
119	71	15	8	183	122	17	13
138	136	21	17	171	224	21	19
147	178	21	11	197	149	23	18
206	155	16	19	143	107	21	11
130	222	11	23	160	135	16	22
160	214	15	15	164	172	16	18
141	99	13	21	209	134	12	10
134	138	8	15	156	127	15	15
95	139	13	14	185	179	25	20
143	119	19	17	199	147	17	12
100	149	22	7	178	166	16	26
120	175	12	12	177	213	12	11
84	160	16	17	236	174	17	19
97	176	13	15	126	201	16	33
92	105	7	12	175	238	27	21
120	136	11	11	199	93	31	21
131	110	11	9	204	256	27	17
143	100	15	12	153	138	15	11
138	147	18	12	206	134	7	18
121	108	15	21	182	133	17	18
187	99	13	11	125	176	15	17
151	130	13	12	108	139	13	19
194	187	8	11	202	243	9	19
106	106	26	15	101	199	17	22
69	104	9	20	140	172	19	21
118	96	8	17	127	154	24	17
114	101	11	17	142	142	24	23
195	105	13	12	198	239	12	19
91	275	13	21	224	186	11	13
186	148	11	16	139	208	19	15
179	171	8	15	239	274	12	17
----------	----------	----------	----------	152	284	16	32
----------	----------	----------	----------	165	204	11	15
----------	----------	----------	----------	147	242	11	12
----------	----------	----------	----------	120	373	----------	----------
----------	----------	----------	----------	105	137	----------	----------

6.4. Pitch determination

Using SEM, cross-section images of prepared CNC films were done, and the values for pseudolayer pitch measured using ImageJ software. The images used are represented in Figure 6.10 – Cross-section images of prepared CNC films, used to determine pitch values The values measured for P/2 are present in Table 6.3.

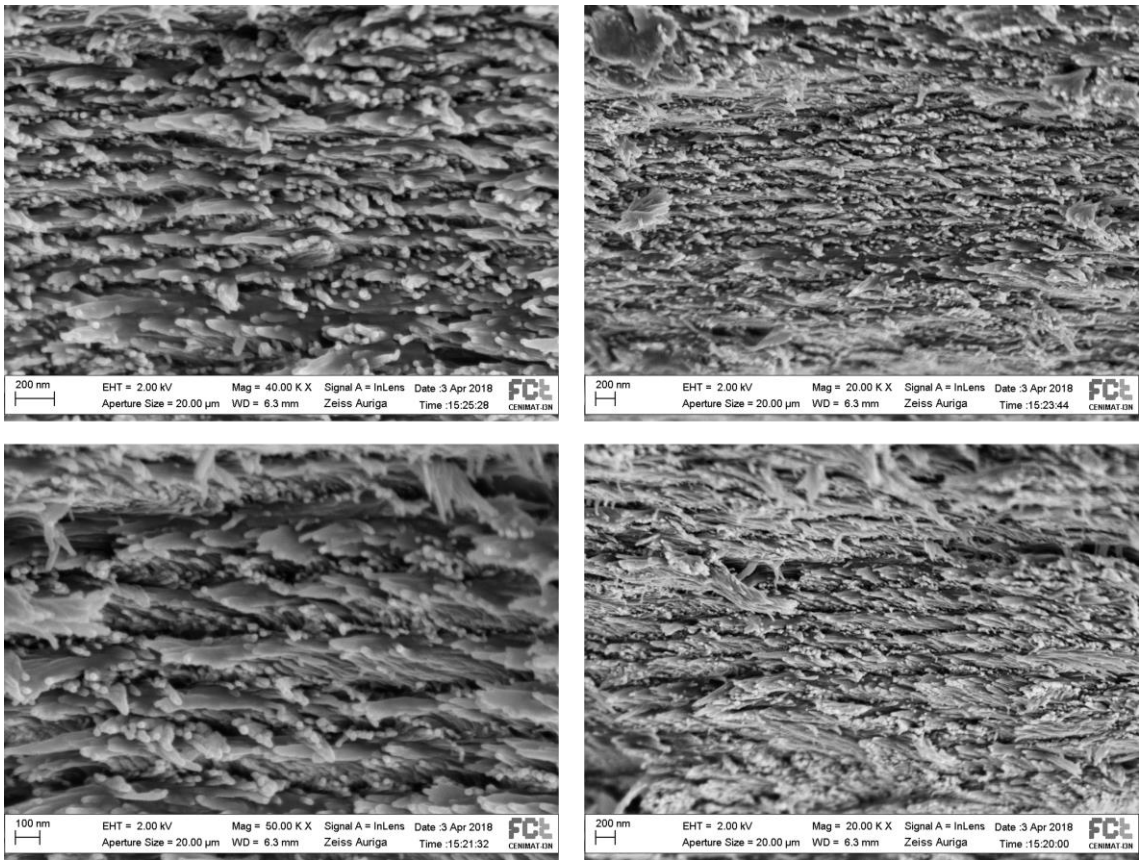

Figure 6.10 – Cross-section images of prepared CNC films, used to determine pitch values

Table 6.3 –Half pitch values measured from SEM images of CNC film cross-sections used to determine maximum reflected light wavelength.

P/2 (nm)			
171	159	218	218
176	181	188	192
171	156	167	200
218	167	170	192
165	167	163	207
218	215	215	178